The compositional evolution of differentiated liquids from the Skaergaard Layered Series as determined by geochemical thermometry

A. A. Ariskin

Vernadsky Institute of Geochemistry and Analytical Chemistry, Russian Academy of Sciences

Abstract. Based on the COMAGMAT-3.65 crystallization model a set of phase equilibria calculations (called geochemical thermometry) have been conducted at $P=1$ kbar and closed conditions with respect to oxygen for 65 rocks representing the principle units of the Layered Series of the Skaergaard intrusion. It allowed us to define the range of initial temperatures (1145 to 1085°C) and oxygen fugacities (1–1.5 log units above QFM to slightly below QFM) of the original crystal mush from which the rocks from LZa to UZa crystallized. In parallel, average major-element compositions of residual (interstitial) liquid were calculated demonstrating a trend of continual enrichment of FeO* (up to ~18 wt.%) and TiO$_2$ (up to ~5.5 wt.%) with only minor variations in the SiO$_2$ contents (48 to 50 wt.%). Projection of the compositions onto the $OLIV$-CPX-QTZ diagram provides evidence that most of the Layered Series crystallized on the Ol-Pl-Cpx-oxide cotectic. Systematic differences between the calculated residual liquid compositions for LZa/LZb and LZc to UZa (which are unlikely to reflect fractional crystallization) are within the accuracy of the COMAGMAT model, but may be also indicative of a late-stage process involving migration and re-equilibration of interstitial liquids. Estimated amounts of interstitial melts trapped in the Skaergaard "cumulates" range around 50 wt.%. Wager's compositions inferred from simple mass-balance were found to lie too far from the Ol-Pl-Cpx boundary to represent a realistic approximation of the low-pressure Skaergaard magma evolution. The main problem of genetic interpretations of the Skaergaard intrusion is a strong misbalance between the parental compositions followed from contact rocks and the results of geochemical thermometry and that of the whole differentiated body. It is most apparent for TiO$_2$ and P$_2$O$_5$ which are almost twice as high in the average intrusion composition compared to the proposed parents. Moreover, the intrusion composition has of 2–4 wt.% less SiO$_2$ and much more iron. One possible explanation is to assume the Skaergaard magma came to the chamber with an amount of crystals ($Ol + Pl$) equilibrated with the calculated parental liquid. However, even if some amount of "hidden" troctolitic material exists, it is unlikely that crystallization in a closed system could produce large volumes of rocks rich in Fe-Ti oxides without complementary more felsic differentiates.

1. Introduction

Investigations of differentiation of the Skaergaard magma have played a special role in igneous petrology by providing a canonical example of the evolution of a tholeiitic magma that had strong iron enrichment and depletion in SiO$_2$ in the middle stages of differentiation. Excellent, unweathered exposures, detailed sampling, and favorable spatial relations
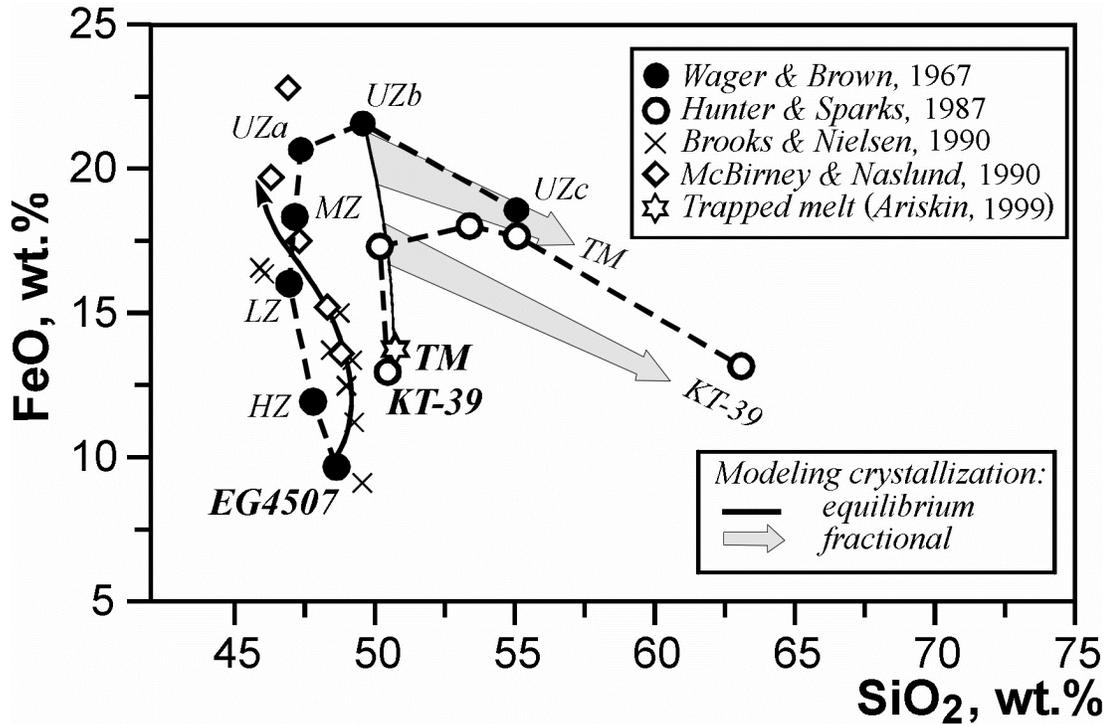
Figure 1. Magmatic differentiation trends proposed for the Skaergaard intrusion. "Natural" trends are based on mass-balance calculations [*Hunter and Sparks,* 1987; *Wager and Brown,* 1967], dike rock compositions [*Brooks and Nielsen,* 1978, 1990], and results of melting experiments [*McBirney and Nakamura,* 1973; *McBirney and Naslund,* 1990]. Zones and subzones are shown next to the relevant symbol: *HZ,* Hidden zone (after 35% assumed crystallization); *LZ,* lower zone (76%); *MZ,* middle zone (88.2%); *UZ,* upper zone (UZa, 95.7%; UZb, 98.2%; UZx c, 99.3%). Calculated crystallization trends represent phase equilibria modelling with COMAGMAT-3.5 at $P = 1$ atm and QFM [*Ariskin,* 1999]: *TM* is the initial "trapped" melt obtained at 1165°C as a result of geochemical thermometry of MBS rocks (Table 1); *EG*4507 and *KT*-39 are the chilled gabbros [*Hoover,* 1989; *Wager and Brown,* 1967].

between the main differentiated units have made it an ideal testing ground for a variety of petrologic concepts and techniques. Based on the premise that the initial Skaergaard magma was a pure liquid free of crystals, with the volumes of the differentiates assumed to be proportional to their thickness in the central part of the intrusion, *Wager and Deer* [1939] proposed a simple graphic technique for the calculation of the composition of the Skaergaard magma at successive stages of differentiation. These early estimates used primarily mass-balance relations between an initial composition inferred from a sample from the chilled margin and average compositions of the main units of the Layered Series. In order to achieve a satisfactory mass balance, *Wager* [1960] had to postulate a large "Hidden Layered Series". The rocks of the Upper and Marginal border series were not included in the calculations, with the Sandwich Horizon being taken to be the final product of differentiation. The result was a series of compositions that became progressively more iron- rich and silica-poor throughout almost the entire sequence of differentiation [*Wager and Brown,* 1967]. Silica increased measurably at the very end when it reached a maximum value of about 55 wt.% with 18.5 wt.% FeO in the extreme differenti-

ate (Figure 1). Subsequent investigations revealed two serious flaws in Wager's calculations. First, the *EG*4507sample of the chilled margin used for the initial magma was shown to be contaminated by metamorphic country rocks and therefore unrepresentative of the original liquid [*Hoover,* 1989; *McBirney,* 1975]. Second, a geophysical survey showed that the huge Hidden Zone required by the mass balance does not exist [*Blank and Gettings,* 1973]. These observations do not necessarily invalidate the main conclusion that the differentiated liquid became increasingly iron-rich throughout essentially the full range of differentiation, but one must take into account two additional circumstances. (1) The principal uncertainty in calculating Skaergaard liquid compositions by mass-balance is the proportions of the individual units of the Layered and Border Series. Although their thickness can be measured, it is difficult to determine their original lateral extent and volume: one can obtain a range of compositional trends simply by using different relative volumes. (2) Any trend calculated by mass-balance must be consistent with phase equilibria constraints if this trend is assumed to have resulted from magmatic fractionation controlled by crystal-melt equilibria. However, attempts to deduce the Skaergaard

Table 1. Compositions of chilled gabbros and trapped liquids proposed to be parental to the Skaergaard igneous rocks

Sample	Chilled gabbro		Trapped liquids		
	*EG*4507	*KT*-39	*LA*-95 (LZa) 1150°C	*EC*-22 (MBS) 1160°C	*TM* (MBS) 1165°C
SiO_2	48.58	50.46	51.44	51.30	49.94
TiO_2	1.18	2.70	1.61	1.61	1.68
Al_2O_3	17.40	13.41	13.03	12.99	12.93
FeO_{tot}	9.73	12.96	13.59	13.55	13.22
MnO	0.16	0.22	0.26	0.26	0.19
MgO	8.71	6.71	6.15	6.13	6.89
CaO	11.50	10.34	11.18	11.15	12.38
Na_2O	2.39	2.41	2.38	2.37	2.37
K_2O	0.25	0.57	0.28	0.28	0.26
P_2O_5	0.10	0.22	0.09	0.09	0.15

Note: Natural samples: *EG*-4507 [*Wager and Brown*, 1967], *KT*-39 [*Hoover*, 1989]. Experiments at *QFM* buffer: LA-95 denotes a glass after melting the rock from LZa [*McBirney and Nakamura*, 1973; *McBirney and Naslund*, 1990]; *EC*-22 denotes a glass after melting the rock from MBS [*Hoover*, 1989]. Phase equilibria calculations (geochemical thermometry): *TM* represents an average for 6 liquid lines of descent intersected at 1165°C [*Ariskin*, 1999]. All compositions are normalized to 100 wt.%.

liquid compositions from mass-balance calculations based on phase equilibria constraints [*Hunter and Sparks*, 1987] and magma crystallization models [*Ariskin*, 1999; *Ariskin et al.*, 1988] drew attention to serious contradictories of the empirically constructed trends which seemed to be inconsistent with experimentally-determined modal mineral proportions.

Hunter and Sparks [1987] used a modified version of Wager's calculations. They emphasized that at 48.1 wt.% SiO_2 in the sample *EG*4507 ($\approx$ initial magma) the monotonous silica depletion trend can not be consistent with the low SiO_2 contents (44–46%) of the observed "gabbroic assemblage" *Ol-Pl-Aug* $\pm$ *Mt*. Another discrepancy was that the composition at which the iron enrichment changed to silica enrichment did not coincide with the onset of Fe-Ti oxides crystallization in the rocks, which are known to appear quite early in the Skaergaard Layered Series [*McBirney*, 1989; *Wager and Brown*, 1967]. Following this reasoning, *Hunter and Sparks* [1987] argued that the evolution of the Skaergaard magma was similar to that seen in differentiated tholeiitic lavas of Iceland and western Scotland. These speculations were supported by simple mass-balance calculations, including subtraction of specified amounts of the Skaergaard gabbroic components from the composition of chilled gabbro *KT*-39 assumed to present more accurate the estimate of the Skaergaard parental magma [*Hoover*, 1989]. The rhyolitic end-product was said to have been erupted without leaving a trace in the presently exposed body of Skaergaard rocks. The geological aspect of the proposed interpretations found little support among petrologists who had worked on the intrusion and were familiar with the field relations [*Brooks and Nielsen*, 1990; *McBirney and Naslund*, 1990; *Morse*, 1990]. They objected that Hunter and Sparks had forced the Skaergaard liquids to follow the trend observed in volcanic rocks by assuming unrealistic volumetric proportions and ignoring well-documented geologic evidence. This was the main reason for rejecting the revised direction of the Skaergaard magma fractionation, although the phase equilibria problems were left unresolved [*Ariskin*, 1998; *Hunter and Sparks*, 1990].

1.1. Modelling Fractional Crystallization

An indirect way to define compositional evolution of the Skaergaard magma is to calculate perfect fractionation trajectories for a liquid thought to be parental to the whole intrusion. Recent calculations with the use of COMAGMAT-3.5 program including more accurate models for the simulation of *Mt* and *Ilm* crystallization [*Ariskin and Barmina*, 1999] confirm the conclusion [*Ariskin et al.*, 1988; *Toplis and Carroll*, 1996] that in systems open with respect to oxygen *Mt* saturation leads to strongly decreasing iron and increasing silica contents of residual liquids, whereas closed systems crystallize lowered amounts of magnetite with a less pronounced iron depletion in the liquid. These simulations were conducted for two initial compositions – *KT*-39 [*Hoover*, 1989] and *TM* [*Ariskin*, 1999]. The latter is an average composition of six modelled melts assumed to be trapped in the most primitive rocks of the Marginal Border Series (Table 1). The phase equilibria calculations give evidence that both compositions are subcotectic (*Ol* + *Pl*), with *KT*-39 slightly oversaturated with *Ol*, whereas *TM* is closer to the *Ol* + *Pl* + *Aug* saturation. Liquid lines of descent representing the fractionation at 1 atm and *QFM* are plotted in Figure 1. Each of the initial compositions is shown by two evolutionary lines: the upper ones include calculations without any corrections in COMAGMAT-3.5, whereas the lower lines represent a corrected model, providing a maximally possible compositional shift based on the accuracy of the *Mt*- and *Ilm*-models. With these uncertainties [*Ariskin*, 1999] reached the following conclusions: (i) both parents exhibit only minor decrease in SiO_2 as compared to the proposed $FeO-SiO_2$ trend [*Brooks and Nielsen*, 1978, 1990; *Wager and Brown*, 1967]; (ii) all of the calculated trajectories indicate a well-defined inflection point, where the content of SiO_2 starts to increase due to the appearance of *Mt*; (iii) the maximum possible iron enrichment of residual melts is approximately 18 wt.% FeO for *KT*-39 and 20% for *TM*.
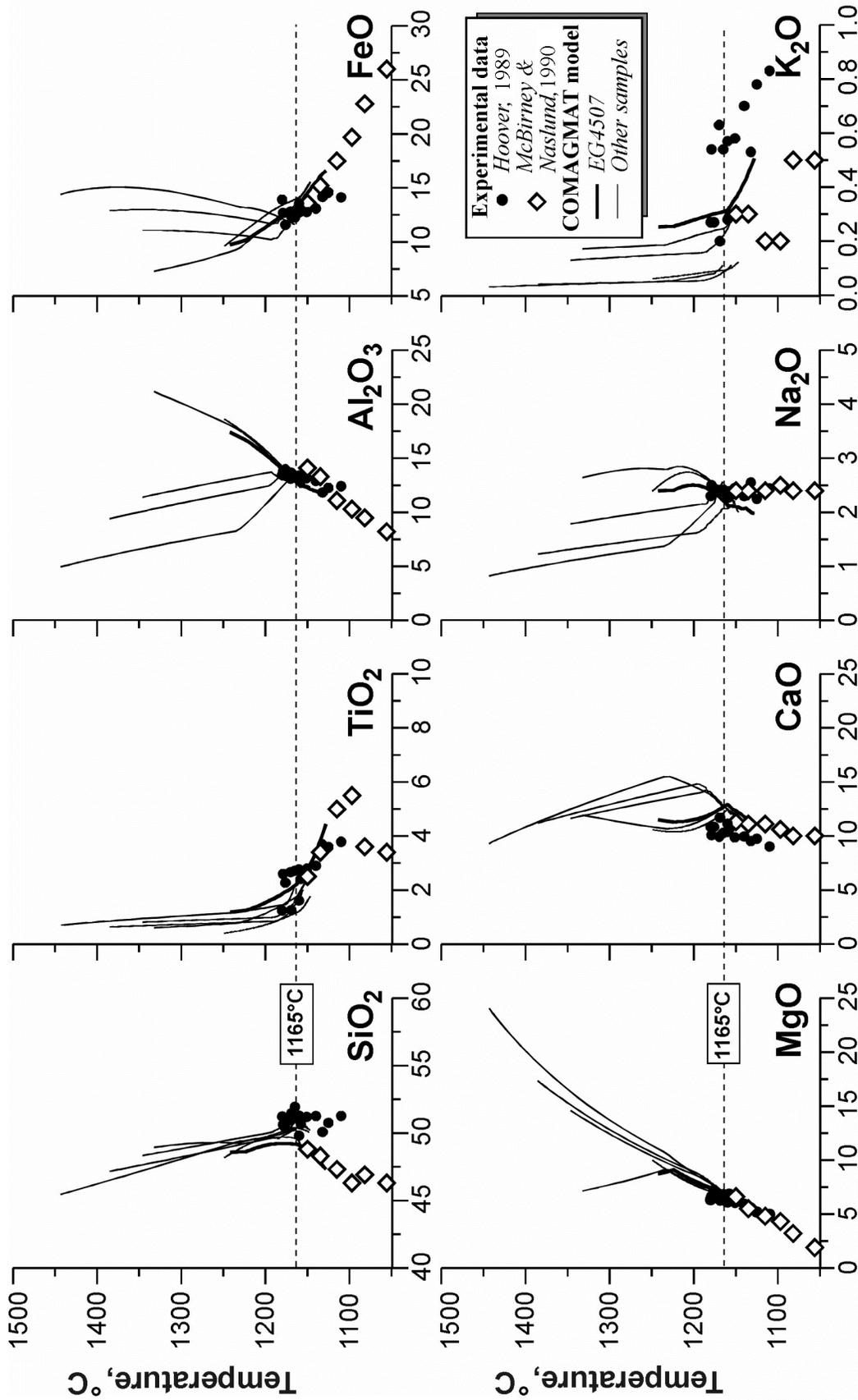
Figure 2. Example of geochemical thermometry for the Skaergaard MBS rocks. Lines correspond to the equilibrium crystallization trajectories calculated at 1 atm and QFM conditions for six contact gabbros; the temperature of 1165±10°C is assumed to indicate the initial temperature for the trapped liquid [*Ariskin,* 1999]. Experimental data: circles are residual liquids for the Marginal Border Series pristine rocks [*Hoover,* 1989]; diamonds are those obtained for the Lower and Middle Layered Series rocks [*McBirney and Nakamura,* 1973; *McBirney and Naslund,* 1990].

Table 2. Average bulk-rock compositions of the principal units of the Layered Series and equivalent rocks of the Marginal Border Series [*McBirney,* 1996]

Unit	LS	MBS	LS	MBS	LS	MBS	LS	MBS	LS	MBS
Zone	LZa	LZa*	LZb	LZb*	LZc	LZc*	MZ	MZ*	UZa	UZa*
SiO_2	48.12	49.43	48.84	50.30	41.10	44.86	42.79	43.46	43.07	44.33
TiO_2	1.35	1.00	1.44	1.08	6.92	4.91	6.79	5.44	5.67	6.24
Al_2O_3	16.81	13.71	12.55	14.13	11.02	11.35	11.53	12.48	11.17	10.05
FeO_{tot}	11.13	11.87	12.84	11.83	21.10	19.02	20.00	20.51	22.52	21.47
MnO	0.16	0.19	0.21	0.18	0.26	0.26	0.26	0.23	0.31	0.29
MgO	9.42	10.77	10.13	9.42	7.61	6.60	6.24	5.64	5.62	5.57
CaO	10.11	10.76	11.57	10.89	9.77	10.59	9.87	9.54	8.62	9.39
Na_2O	2.52	1.93	2.13	1.88	1.97	2.03	2.23	2.24	2.55	2.08
K_2O	0.27	0.25	0.20	0.22	0.20	0.26	0.21	0.35	0.26	0.34
P_2O_5	0.11	0.08	0.09	0.07	0.05	0.13	0.08	0.12	0.22	0.24

Note: LS is the Layered Series, MBS is the Marginal Border Series. Normalized to 100 wt.%.

1.2. Experimental Determination of Trapped Liquid Compositions

Another approach is based on the premise that the Skaergaard gabbros retained a certain amount of trapped or residual liquid within the matrix of cumulus crystals. According to the widely accepted interpretation of layered gabbros as mixtures of the primary minerals and melts, one can estimate the amount of this interstitial component from the bulk-rock concentrations of incompatible elements [e.g., *Chalokwu and Grant,* 1987; *Henderson,* 1970]. By melting a sample to a temperature slightly above to its solidus the interstitial liquid can be restored and analyzed. When this method was used to determine the composition of trapped liquid in rocks of the Layered Series [*McBirney and Nakamura,* 1973], at oxygen fugacities between the QFM and WM buffers and the temperatures lower 1150°C it yielded a series of compositions that follow the "Wager trend" with a steady increase in iron and no pronounced increase of silica [*McBirney and Naslund,* 1990]. In the FeO-SiO$_2$ diagram this experimental trend corresponds well to that followed from some co-magmatic dike compositions (Figure 1).

Hoover [1989] performed several additional melting experiments on gabbros representing the earliest and least differentiated rocks crystallized within the Marginal Border Series. The partial melts obtained at 1160–1180°C and QFM conditions contained markedly more SiO$_2$ and less FeO than the residual liquids observed from "the Layered Series" experiments. In part, the compositional discrepancy may be attributed to the effect of temperature supported by the results of modelling equilibrium crystallization for the chilled gabbro $EG4507$ (Figure 2). One can see, that at low temperatures the modelled $EG4507$ line resembles the silica depletion and iron enrichment trend, satisfying both of the above discussed experiments [*Ariskin,* 1999]. It is noteworthy that at the same temperature the chilled gabbro is characterized by silica contents 1.5 wt.% lower than partial melts of the most of the Marginal Border Series rocks or KT-39 and TM parents. This indicates the possibility that there were differences in the compositions of magmatic liquids parental to marginal rocks and those of presenting the Layered Series cumulates.

1.3. Calculations for the Marginal Border Series

Utilizing the COMAGMAT-3.5 crystallization model and a modelling principle known as "Geochemical thermometry" (Appendix 1), the reconstruction of the intersitial liquid composition has been performed for six samples representing the least evolved part of the Marginal Border Series [*Ariskin,* 1999]. Five of these samples were collected within 1 to 8.5 m of the intrusive contact [*Hoover,* 1989], whereas the sixth was the "chilled marginal gabbro" $EG4507$ [*Wager and Brown,* 1967]. Calculations of equilibrium crystallization at 1 atm pressure, dry conditions and QFM buffer indicated that the mineral crystallization temperatures are correlated with the starting compositions, demonstrating a wide temperature field of Ol for high-magnesia samples and an early crystallization of Pl for a plagioclase-rich rock. Two samples (including $EG4507$) showed sub-cotectic $(Pl + Ol)$ relations in the range 1230–1250°C. In accordance with the sequence of crystallization, the calculated lines of descent yielded an obvious intersection in the range of 1175–1155°C (Figure 2). The temperature of 1165±10°C was accepted as representing the initial temperature of the Skaergaard parental magma. The average liquid composition representing this cluster of six evolutionary lines at 1165°C is given in Table 1. It is close to liquid compositions that *Hoover* [1989] obtained in his melting experiments with marginal rocks. In this paper, estimates of major-element geochemistry for "residual liquids" and primary mineral proportions for the LZ, MZ, and UZ rocks are first presented.

2. Calculations for the Main Skaergaard Units

Before carrying out final geochemical thermometry calculations and a systematic analysis of the modelled liquid lines of descent for real rocks, a set of preliminary simulations of equilibrium crystallization was conducted for the average Layered and Marginal Border Series rocks (Table 2). The *Layered Series* (LS) of the Skaergaard intrusion represents
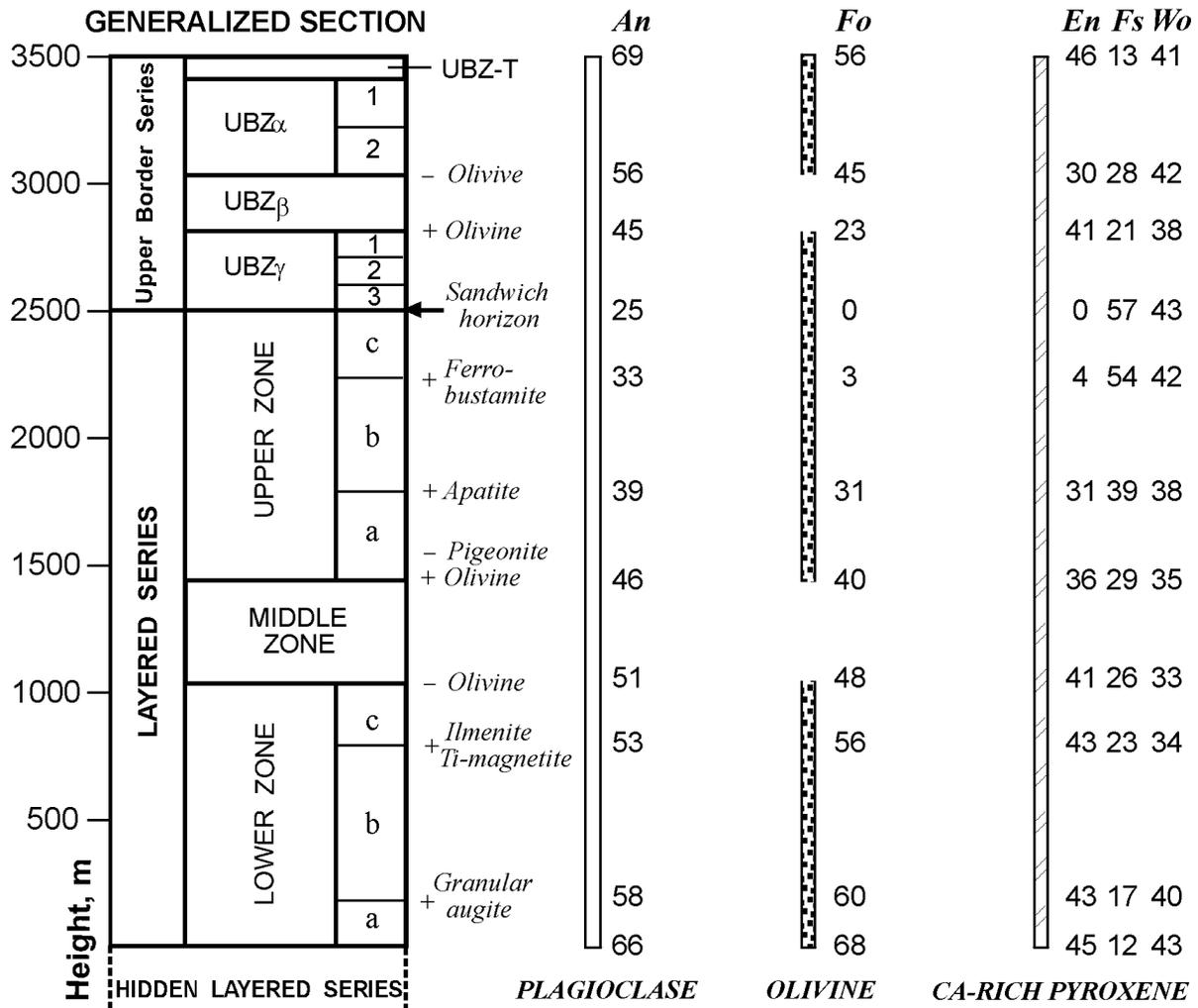
Figure 3. The main units of the Layered Series and the Upper Border Series [*McBirney*, 1996]. The LS zones are defined by the appearance or disappearance of primary phases, or, in the case of LZb, by the transition from the poikilitic form of the Ca-pyroxene to the granular one. The Upper Border Series is divided into three subzones (α, β, and γ) equivalent to the LZ, MZ and UZ. The compositions given for *Ol, Pl,* and *Aug* at zone boundaries are approximate and may vary laterally.

a sequence of rocks that formed from the floor upward. It is lithologically and structurally distinct from the *Marginal Border Series* (MBS) that crystallized inward from the walls and the *Upper Border Series* (UBS) that crystallized downward from the roof. The upper boundary of the LS is defined by its contact with the UBS along a level known as the Sandwich Horizon – SH [*Wager and Deer,* 1939]. As a rule, this level is recognizable in the field by the contrast between the mafic ferrodiorites of the LS and more felsic UBS [*McBirney,* 1989]. In accordance with the nomenclature established by *Wager and Brown* [1967], the Layered Series is divided into *Lower, Middle*, and *Upper Zones* by the disappearance of abundant primary olivine at the base of Middle Zone and by its reappearance at the base of Upper Zone (Figure 3). Olivine is present in Middle Zone only as rare grains and as thin reaction products between pyroxene and Fe-Ti oxides. Lower Zone is further divided into three subzones (LZa, LZb,

and LZc) by the distinctive poikilitic texture of pyroxene in LZa and by the appearance of abundant ilmenite and magnetite at the base of LZc. In a similar way, Upper Zone is divided into three subzones (UZa, UZb, and UZc) by appearance of abundant, coarse apatite at the base of UZb and by the mosaic form of inverted ferrobustamite in UZc. Inverted pigeonite is found in all rocks up to the middle of UZa but is rarely abundant. Interstitial granophyre is common in the upper part of Upper Zone.

These relations dictate the main minerals (olivine, plagioclase, augite, pigeonite, ilmenite, magnetite, and apatite) that should be included in any phase equilibria model used for the LS rocks. At present, the thermodynamic basis of COMAGMAT involves mineral-melt equilibria equations well calibrated only for the first six minerals [*Ariskin and Barmina,* 1999, 2000] and limits its application to LZa through UZa where apatite was not a primary phase.

2.1. Intensive Parameters of Crystallization

Other limitations are imposed by the probable range of intensive parameters of the crystallization. The fortuitous relations of the polymorphs of silica and Fe-rich pyroxenes in the Sandwich Horizon rocks allowed *Lindsley et al.* [1969] to show that that level crystallized at a pressure of 600 ± 100 bars and a liquidus temperature of $970\pm20°C$. Judging from the densities of the overlying gabbros and basalts, this corresponds to a depth of about 2 km for the Sandwich Horizon and places LZa ∼4.5 km and UZa ∼3 km below the original surface [*McBirney,* 1996]. It indicates an initial pressure of ∼1.3 kbar for the LZa and ∼0.9 kbar at the boundary between MZ to UZ. For such low pressures COMAGMAT has been shown to produce accurate phase equilibria calculations [*Ariskin,* 1999; *Yang et al.,* 1996].

Estimates of redox conditions during crystallization are based on mineral equilibria calculations, electrochemical measurements, and results of melting experiments. Thermodynamic calculations for quartz-fayalite-magnetite and magnetite-ilmenite equilibria indicate that the oxygen fugacity at the base of LZa was slightly above QFM [*Frost and Lindsley,* 1992; *Morse et al.,* 1980; *Williams,* 1971] and declined towards MZ, followed by a sharp decrease at UZ which results in as much as QFM-2 at the Sandwich Horizon [*Frost et al.,* 1988]. Although Fe-Ti oxides were shown not to have preserved their original magmatic compositions, these estimates are in fairly good agreement with indirect evidence from experimental studies of phase relations of the natural rocks [*McBirney and Naslund,* 1990]. Measurements of intrinsic fO_2 indicated values ranging from IW-WM [*Sato and Valenza,* 1980] to 0.5–1.5 units above the QFM buffer [*Kersting et al.,* 1989].

Using the compositions of *Ol-Pig-Mt-Ilm* assemblages from the LZc, MZ, and UZa rocks, *Williams* [1971] calculated "frozen" equilibria temperatures of 1150–1050°C, with the highest values representing Lower Zone. This is in general agreement with both previous estimates for the SH (970°C) and those of melting experiments indicating temperatures of 1150–1002°C for partial melts that seem to represent differentiated (residual) liquids from the UZa to UZc [*McBirney and Naslund,* 1990]. Melting of the chilled gabbro KT-39 [*Hoover,* 1989] and results of geochemical thermometry of contact rocks [*Ariskin,* 1999] produced closed temperatures for the initial *Ol-Pl* cotectics of about 1165°C. Attempts to use temperature-sensitive oxide and two-pyroxene equilibria has resulted in under-estimations of the liquidus temperatures due to significant re-equilibration during subsolidus cooling [*Jang and Naslund,* 2001].

2.2. Differences Between Open and Closed to Oxygen Calculations

Calculations for the average Layered and Marginal Border Series rocks were carried out at total pressure $P = 1$ kbar, 0.1 wt.% H_2O in the melt, and oxygen buffered conditions (QFM+1 to QFM−2), using a revised COMAGMAT model (version 3.65) which allowed us to calculate low-temperature relations near 1100°C more accurately than could be done with COMAGMAT-3.5 (Appendix 2). This is critically important because only the lowermost rocks of the LZa an LZb zones fall within the range of experimental glasses used in the calibrations of COMAGMAT, whereas the LZc, MZ, and UZa rocks are too depleted in SiO_2 and enriched with FeO because of their abundant Fe-Ti oxides (Figure 4d). I draw attention to this fact because of the validity of genetic conclusions based on the COMAGMAT-3.65 calculations depends strongly on the accuracy of phase equilibria extrapolations to the low-silica field, including estimates of the arrival of *Ilm* and *Mt* [*Ariskin and Barmina,* 1999].

A general impression of the calculated trajectories can be obtained from Figure 5, where results of the phase equilibria modelling at QFM are shown. Note that all the calculations were conducted up to 80% crystallized (20% of residual liquid), as marked in the figure by thin solid (LS) and dashed (MBS) lines at the lowest temperatures for each computation. These plots demonstrate both common features and principal differences between the temperature sequences calculated for the main Skaergaard units. There is a general correspondence between the LS rocks and their MBS equivalents in the order of minerals crystallized at each horizon, which is in good agreement with the assumption that two series crystallized at the same time from the same magma (Figure 5). The composition of LZa indicate subcotectic crystallization of $Ol + Pl$, followed by Aug and, at a late stage, little if any Ilm. The LZb sequences indicate a large expansion of the field of high-Ca pyroxene, as is consistent with the appearance of abundant granular Aug crystals that characterize that zone, whereas the LZc trajectories are marked by the early appearance of both Ilm and Mt. Similar phase relations were obtained for the MZ and UZa rocks (including their MBS equivalents), with the exception that Ol was found to be dissolved completely at a late stage (see below). It is interesting that the Pig field is noticeably wider in the marginal rocks, with the result that Ol disappears earlier owing to its reaction with residual liquids. It is certainly correlated with higher contents of SiO_2 in the Marginal Border Series equivalents (Table 2) and may be indicative of the principal compositional differences between the liquids "trapped" in the MBS and the Layered Series rocks [*Ariskin,* 1999]. The oxide-rich gabbros of the Layered (LZc→UZa) and the Marginal Border Series (LZc* →UZa*) demonstrate almost simultaneous precipitation of ilmenite and magnetite, with Ilm crystallized slightly earlier in the LS rocks as 33 compared to MBS. Note, also, that the MBS oxide-rich types seem to have lower-temperature assemblages than those of the Layered Series at the same crystallinity. This latter observation seems to support ideas that the LS has been formed from a liquid that had already crystallized on the wall.

The modelled disappearance of Ol at 1100°C in the MZ and MZ* equivalents corresponds well to the absence of olivine within these units (Figure 3), but the relatively early disappearance of the mineral obtained for the UZa and UZa* average compositions (Figure 5) is inconsistent with the petrographic character of these Ol-bearing units. This must be considered the most significant disagreement of the calculations with the natural observations. In an attempt to resolve the problem we performed an additional set of 20
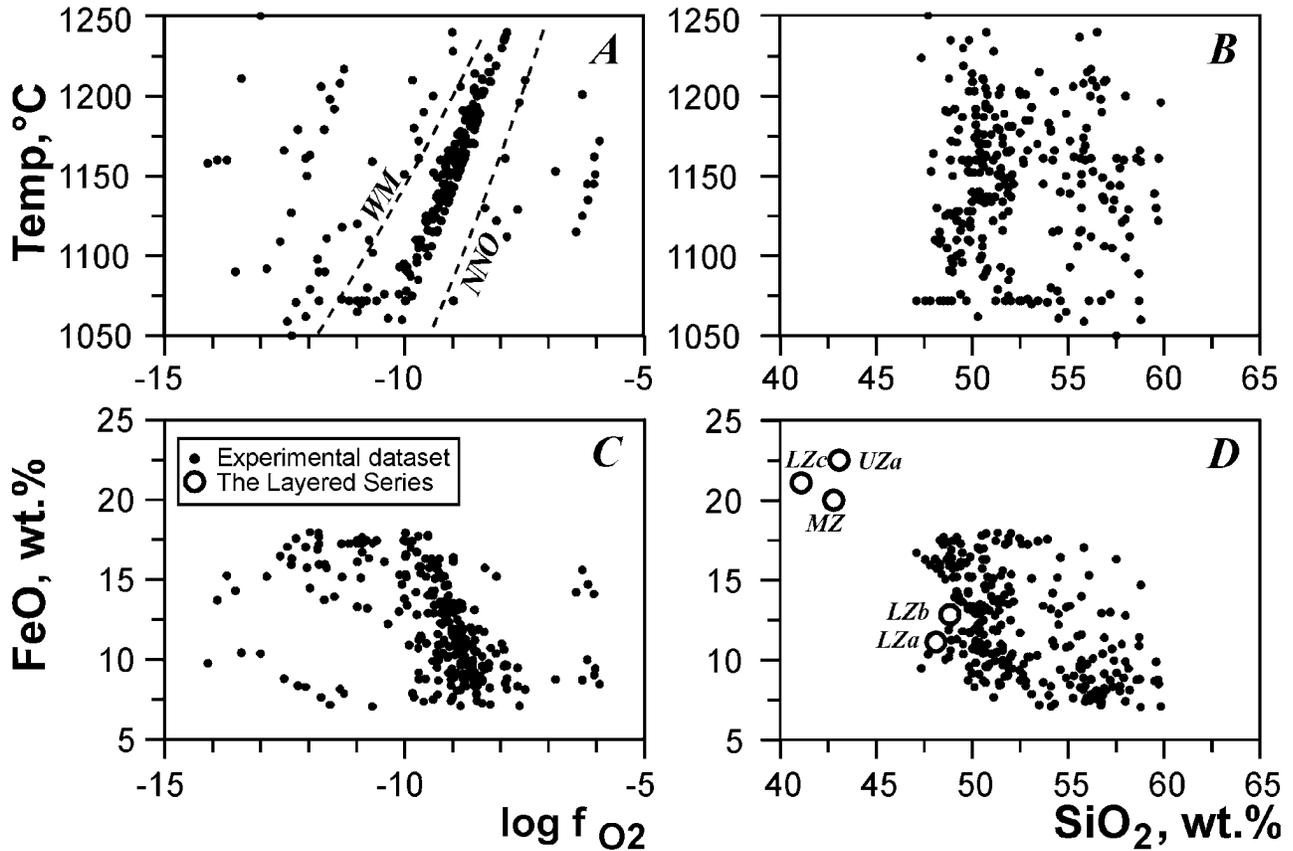
Figure 4. Experimental conditions and compositional characteristics of glasses used in the recalibration of the COMAGMAT model (see Appendix 2). The range of temperatures and FeO contents in experimental glasses: **A, C** as a function of oxygen fugacity; **B, D** in terms of SiO_2 contents. Run duration ≥ 48 hours. Extracted from the INFOREX experimental database [*Ariskin et al.,* 1996, 1997]. In the FeO-SiO_2 diagram the average bulk-rock compositions of the Layered Series units are shown for comparisons, see Table 2.

calculations simulating the course of equilibrium crystallization at closed-to-oxygen conditions, using the average LZa, LZb, LZc, MZ, and UZa bulk-rock compositions. These trajectories were calculated at $P = 1$ kbar and 0.1 wt.% H_2O, with the initial $Fe^{3+}/(Fe^{3+}+Fe^{2+})$ ratios in the melt ranging from 0.10 to 0.25. Some of the results are shown in Figure 6. They include comparisons of the "closed" modal proportions with those obtained in the "open" (QFM) systems. The basic relations are presented here as a function of the total crystallinity with the amount of the residual liquid given as the ordinate. Such a presentation allows one to visualize the changes in phase proportions between the minerals and melt, as equilibrium crystallization proceeded.

2.3. Changes in Phase Proportions of Silicate Minerals and Fe-Ti Oxides

The closed system calculations indicate olivine to be a stable phase, at least up to a crystallinity of 80%, with the LZc and UZa equivalents characterized by a significant increase in the modal Ol proportion at late stages. This is

certainly correlated with the decline of Pig stability relative to those observed in the QFM buffered systems (Figures 5, 6). In fact, the dissolution of Ol is typical of both "open" and "closed" calculations that show an inflection in olivine proportions just after the appearance of magnetite (the later appearance of Pig reinforces the dissolution). It may indicate a peritectic reaction in the iron-enriched basaltic systems, such as: $Ol + l \rightarrow Aug(\pm Pig) + Mt(\pm Ilm) \pm Pl$. The effects of this reaction on phase and chemical relations have commonly been observed in phase equilibria calculations since the end of 1980's [*Ariskin and Barmina,* 2000; *Ariskin et al.,* 1988]. Petrological signatures of similar peritectic relations are documented in the Skaergaard rocks as thin rims of olivine produced by reaction between pyroxene and Fe-Ti oxides [*McBirney,* 1996]. As shown in Figure 6, the Pig field is wider in UZa than it is in UZc. It is correlated with higher average contents of SiO_2 ($\sim$43.1 against 41.1 wt.%), even though the Upper Series rocks are richer in FeO ($\sim$22.5 against 21.1 wt.%, Table 2). This may be explained by: (i) a higher activity of SiO_2 in the residual liquid, or (ii) a greater amount of residual liquid in the UZa rocks. Results of geochemical thermometry given below sup-
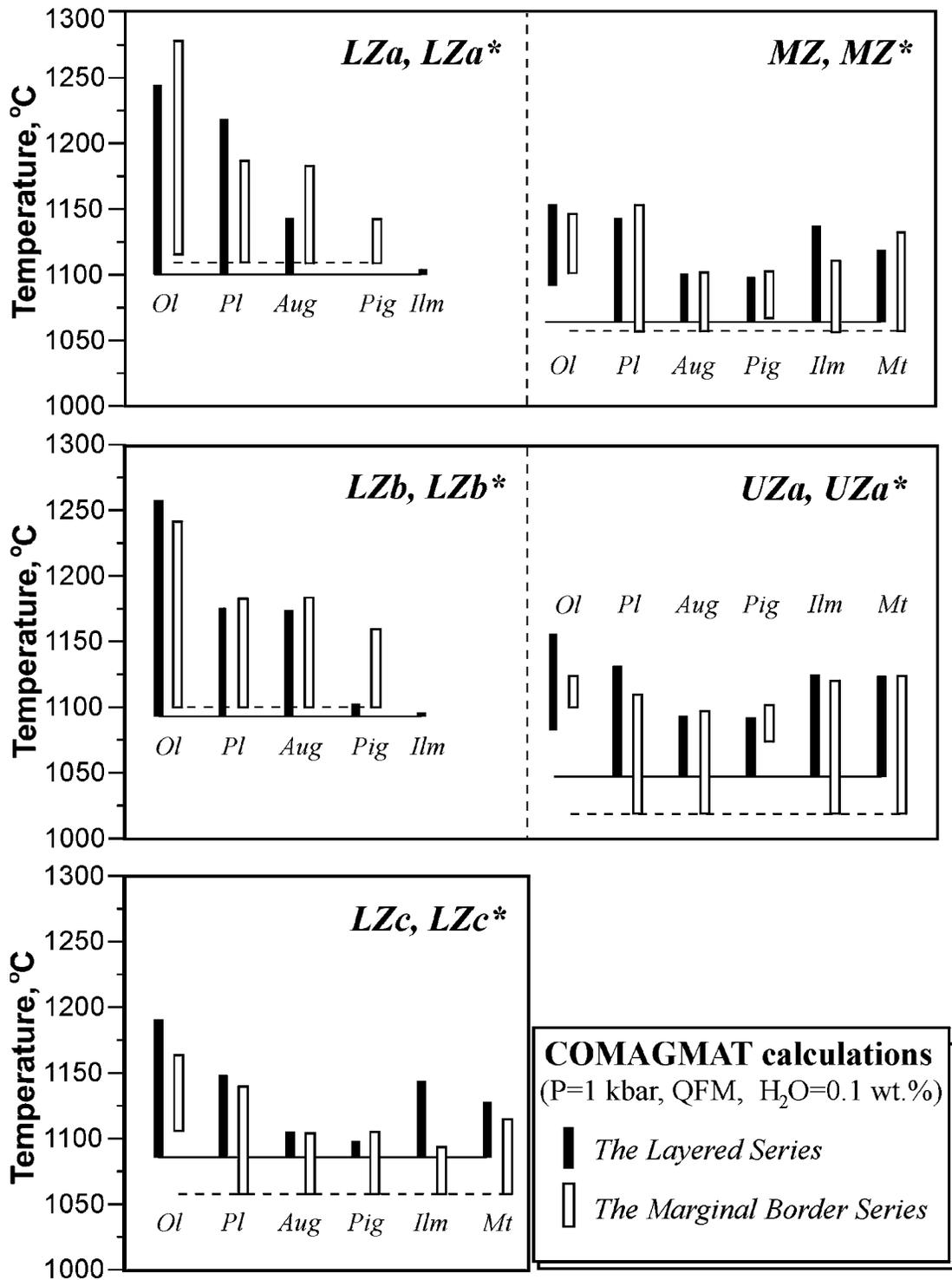
Figure 5. Mineral crystallization sequences modelled for the average bulk-rock compositions of the principal units of the Layered Series and equivalent rocks of the Marginal Border Series (Table 2). Calculations of equilibrium crystallization using the COMAGMAT-3.65 program at P=1 kbar, 0.1 wt.% H_2O in the starting melt, and redox conditions corresponding to the QFM buffer.
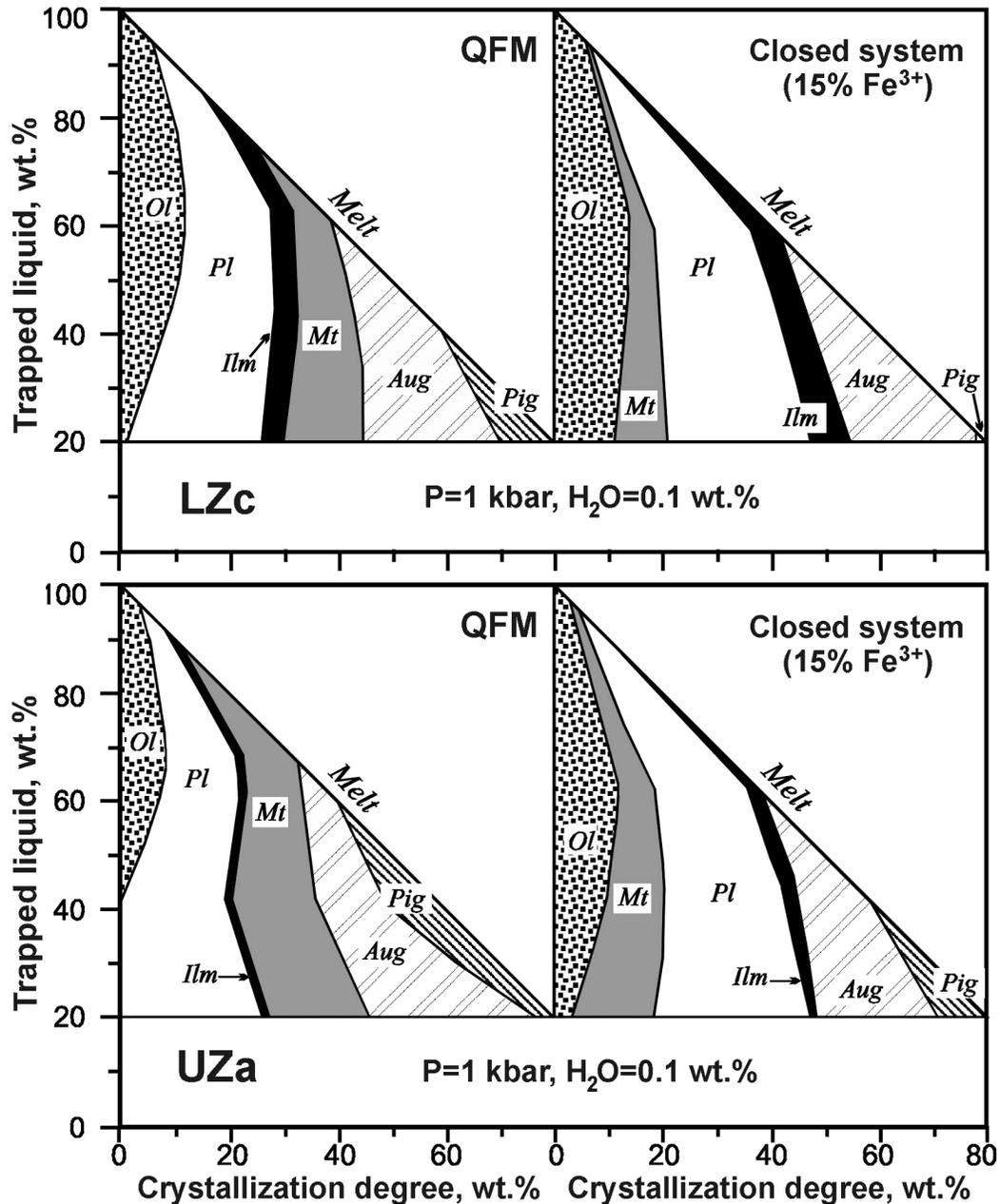
Figure 6. Evolution of phase proportions in the crystallized melts corresponding to the average bulk-rock compositions of the LZc and UZa subzones. Calculations of equilibrium crystallization were carried out using COMAGMAT-3.65 at P=1 kbar and 0.1 wt.% H_2O: open systems correspond to the QFM buffer; closed systems are defined by $Fe^{3+}/(Fe^{3+}+Fe^{2+}) = 0.15$ in the starting melt.

port the first explanation, but it should be noted that the observed reappearance of *Ol* in UZa was followed closely by the disappearance of Ca-poor pyroxene at about the same level as the appearance of greater amounts of interstitial granophyre [*McBirney,* 1996].

The results have an important bearing on the modal proportions of Fe-Ti oxides. The proportions of *Mt* calculated by COMAGMAT-3.65 in the systems closed to oxygen are two-thirds of those calculated at open conditions (Figure 6).

This is not surprising, because of the effect has been demonstrated experimentally [*Osborn,* 1959; *Presnall,* 1966] and confirmed by phase equilibria calculations [*Ariskin et al.,* 1988; *Ghiorso and Carmichael,* 1985; *Toplis and Carroll,* 1996]. A more informative approach is to analyze changes in the modal proportions of ilmenite. At closed conditions an increase in the *Ilm* proportion is observed, so that the bulk *Ilm/Mt* ratio shifts in favor of ilmenite (Figure 6). This suggests that closed-system crystallization more realistically re-
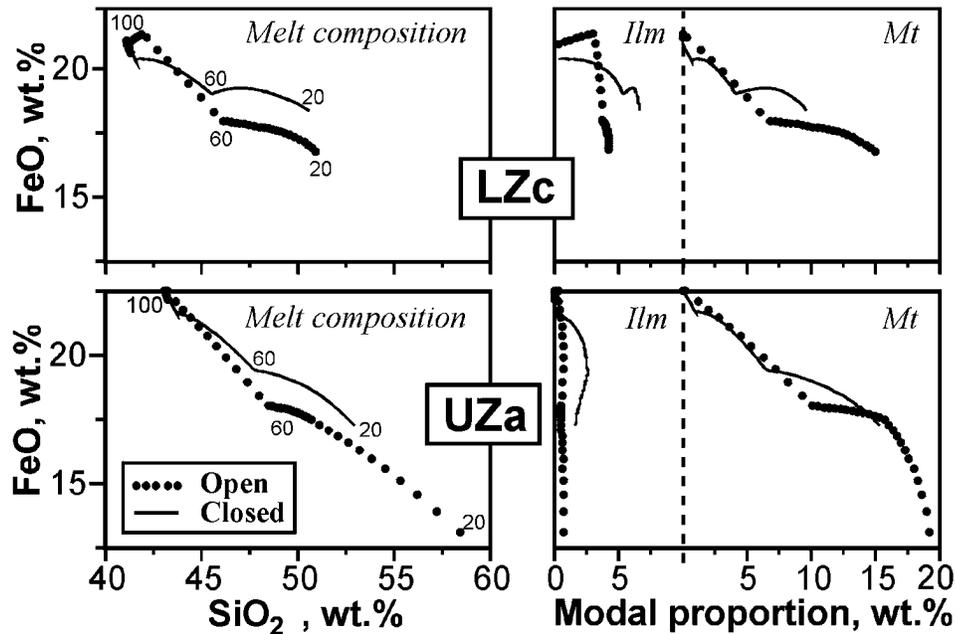
Figure 7. Covariation of FeO and SiO$_2$ in the residual liquids in comparison with modal proportions of Fe-Ti oxides calculated for equilibrium crystallization of the LZc and UZa initial compositions. Results are given for conditions both open and closed with respect to oxygen (same as shown in Figure 5). Numbers next to the calculated lines denote the calculated amount of residual liquid.

produces the observed relations, since ilmenite is more abundant than magnetite in the Skaergaard rocks [*McBirney*, 1989]. The simultaneous crystallization of both oxides from the LZc and UZa melts may be explained from experimental results of *Snyder et al.* [1993]. These authors demonstrated that for a closed iron and titanium enriched system, *Ilm* precipitation results in the increase of $Fe^{3+}/(Fe^{3+}+Fe^{2+})$ in the melt, driving the liquid into the *Mt* stability field. Crystallization of magnetite has the opposite effect depleting the residual melt in Fe_2O_3 and lowering the relative fO_2 value, so that the liquid is quickly driven into the *Ilm* field. The COMAGMAT calculations are also consistent with this observation (Figure 6).

In determining liquid compositions it is also important to estimate the effect of changing modal mineral proportions on the calculated liquid lines of descent, specifically the trend of SiO$_2$ versus FeO. The main differences in the liquid evolution for systems open or closed to O2 are shown in Figure 7, where the modelled T-X trajectories are compared with the corresponding modal proportions of *Mt* and *Ilm* (the same results as shown in Figure 6). Covariations of FeO and SiO$_2$ show that regardless of the initial composition (LZc or UZa) and redox conditions, the early precipitation of Fe-Ti oxides results in a sharp enrichment of the liquid in SiO$_2$ accompanied by decreasing FeO* contents. The rate of iron depletion is less pronounced for the case of the closed system owing to the lower proportion of magnetite crystallized at closed conditions. The amount of *Mt* is limited chiefly by the bulk $Fe^{3+}/(Fe^{3+}+Fe^{2+})$ ratio of the initial melt. In contrast, the calculations for QFM-buffered conditions assume stepwise oxidation of Fe^{2+} to Fe^{3+} in the melt as a result of a con-

tinual transfer of oxygen into the crystallizing assemblage.

I also draw attention to the percent melt shown next to the calculated trends (Figure 7). It is clear that the main objective of interest is in the range of 20 to 60% of the remaining liquid, which corresponds to the expected original modal proportions of cumulus grains (primocrysts) of 80 to 40 wt.%. For the case of the initial composition of LZc, one can see small but real differences of the iron contents of the melt at silica contents of 46 to 50 wt.% SiO$_2$: 19–20 wt.% FeO at closed conditions and 17 to 18 wt.% at QFM. The simulations of UZa at QFM have a much wider range of liquids evolving towards somewhat unusual ferroandesitic compositions containing as much as 13 to 14 wt.% FeO at 60 wt.% SiO$_2$. Nevertheless, the UZa trend for closed conditions falls in a more realistic range of 47.5 to 52.5% SiO$_2$ with 18 to 20% FeO. These results may indicate that our estimates of the differentiated liquid compositions could be best for the LZa and LZb rocks (where primocrysts of oxides are absent). If so, they could provide a good approximation for LZc (and possibly MZ) but yield an approximate composition for the UZa rocks, for which accurate estimates of the initial fO_2 values and bulk $Fe^{3+}/(Fe^{3+}+Fe^{2+})$ ratios are necessary.

Thus, the preliminary calculations indicate complex relations between modal proportions of silicate and oxide minerals, residual liquid compositions, and redox conditions. In general, at relatively oxidizing conditions ($> QFM$) one would expect early precipitation and larger proportions of *Mt* resulting in the pronounced increase in the silica with a complementary depletion in FeO in the melt. Sharply increasing SiO$_2$ causes *Ol* dissolution to occur after the ap-

Table 3. Compositions of differentiated liquids and rock-forming minerals calculated for the principal units of the Layered Series

Zone	LZa ($n = 6$)	LZb ($n = 14$)	LZc ($n = 9$)	MZ ($n = 17$)	UZa ($n = 8$)
Temp, °C	1145	1125	1100	1090	1085
$\log fO_2$	-7.5 ± 0.6	-7.4 ± 0.7	-8.9 ± 0.4	-9.8 ± 0.4	-10.3 ± 0.6
	Residual liquid compositions, wt.%				
SiO_2	49.26 ± 0.76	50.06 ± 1.25	48.04 ± 1.49	49.05 ± 0.86	50.31 ± 1.05
TiO_2	2.50 ± 0.58	2.83 ± 0.76	5.50 ± 0.63	5.25 ± 0.40	4.68 ± 0.24
Al_2O_3	12.74 ± 0.23	11.97 ± 0.77	10.26 ± 0.92	10.35 ± 0.90	11.05 ± 0.31
FeO	14.84 ± 0.81	15.73 ± 0.72	17.05 ± 0.73	17.50 ± 0.55	17.31 ± 0.58
MnO	0.20 ± 0.01	0.21 ± 0.04	0.22 ± 0.04	0.23 ± 0.04	0.24 ± 0.02
MgO	6.29 ± 0.23	5.56 ± 0.32	4.82 ± 0.26	4.00 ± 0.18	3.35 ± 0.19
CaO	11.02 ± 0.54	10.27 ± 0.59	11.00 ± 1.16	10.20 ± 0.78	9.01 ± 0.50
Na_2O	2.59 ± 0.32	2.73 ± 0.34	2.57 ± 0.34	2.80 ± 0.40	3.40 ± 0.29
K_2O	0.39 ± 0.07	0.42 ± 0.22	0.38 ± 0.17	0.39 ± 0.16	0.49 ± 0.14
P_2O_5	0.17 ± 0.06	0.22 ± 0.12	0.15 ± 0.06	0.21 ± 0.15	0.17 ± 0.06
	Equilibrium mineral compositions, mole %				
Ol	Fo (74.9 ± 1.5)	Fo (72.1 ± 2.1)	Fo (64.0 ± 1.5)	See notes	Fo (52.5 ± 2.5)
Pl	An (66.3 ± 1.9)	An (61.9 ± 2.1)	An (57.4 ± 2.1)	An (54.2 ± 2.9)	An (48.0 ± 3.1)
		En (47.0 ± 1.4)	En (42.2 ± 1.8)	En (39.5 ± 1.1)	En (38.0 ± 1.9)
Aug		Fs (13.6 ± 1.3)	Fs (16.8 ± 0.6)	Fs (20.2 ± 0.7)	Fs (22.6 ± 1.0)
		Wo (39.4 ± 0.9)	Wo (41.0 ± 1.7)	Wo (40.5 ± 1.0)	Wo (39.4 ± 1.2)
				En (54.3 ± 1.4)	En (51.4 ± 1.6)
Pig			See notes	Fs (34.1 ± 1.5)	Fs (37.7 ± 1.4)
				Wo (11.6 ± 0.7)	Wo (10.9 ± 0.3)
Ilm			Il (91.4 ± 3.9)	Il (93.8 ± 2.8)	Il (93.7 ± 2.5)
Mt			Ulv (54.0 ± 6.6)	Ulv (72.3 ± 4.9)	Ulv (81.4 ± 6.7)

Note: All of the compositions are average values ($\pm1\sigma$) calculated for the trajectories intersected at a determined temperature, see Figures 9–13. In four cases *Pig* was found to present in the LZc primary assemblage ($En_{59.1\pm0.9}Fs_{29.2\pm0.3}Wo_{11.7\pm0.9}$). In 11 of 16 cases *Ol* was absent in the MZ primary assemblage, however for 5 rocks it was present in the amount of 2–3 wt.% ($Fo_{56.6\pm1.4}$). The *Il* and *Ulv* values represent the $FeTiO_3$ and Fe_2TiO_4 activities calculated using the equations of *Stormer* [1983].

pearance of Ca-rich pyroxene and magnetite, owing to the peritectic reaction discussed above. This process is enhanced by the expansion of the *Pig* stability field resulting from the enrichment with SiO_2 and moderation of the Mg/(Mg+Fe) ratio in the melt [*Grove and Baker,* 1984], leading to the disappearance of olivine at late stages. Under more reduced conditions *Ilm* may crystallize earlier than *Mt*, so that the increase in SiO_2 comes relatively late. In this case the field of *Pig* decreases, whereas the olivine stability field increases (as the result of uncompleted *Ol* dissolution at the same amounts of residual liquid).

Under closed conditions, the *Ol-Pig* relations depend strongly on iron oxidation in the initial melt. At higher $Fe^{3+}/(Fe^{3+}+Fe^{2+})$ values, the *Pig* field is slightly increased because of the enrichment with SiO_2 caused by earlier precipitation of magnetite. The decline of ferric iron is equivalent to melt reduction accompanied by the decrease in the *Mt* crystallization temperature and an expansion of the *Ilm* stability field (Figure 6). The general effect of closed conditions is shown to decrease the total amount of Fe-Ti oxides crystallized, so that the enrichment with SiO_2 and depletion of iron becomes less pronounced (Figure 7). From the results

of phase equilibria calculations one can conclude that only perfectly closed crystallization produces the predominance of *Ilm* over *Mt* observed in the LZc rocks, as well as the preservation of a part of primary *Ol* crystals within the Upper Zone. Note, however, the latter inference is based on the results obtained for relatively oxidized systems with a bulk $Fe^{3+}/(Fe^{3+}+Fe^{2+})$=0.15 (compare Figures 6 and 7). Judging from the liquidus temperatures (Figure 5), it corresponds to an oxygen partial pressure slightly below NNO. Thus, one should not exclude the possibility of more reduced conditions at which the liquid was depleted in SiO_2 so that *Pig* was not crystallized at the late stage, whereas *Ol* continued to crystallize in the Upper Zone.

3. Geochemical Thermometry of the Layered Series Rocks

Geochemical thermometry is a computer-based technique designed to extract initial temperature, interstitial liquid composition, primocryst mineral compositions and modal

proportions, as "recorded" in the whole-rock chemistry [*Frenkel et al.,* 1988a, 1988b]. This approach is based on interpretations of the results of phase equilibria calculations for igneous rocks and their "parents" using the COMAGMAT magma crystallization model [*Ariskin,* 1999], see Appendix 1. Several varieties of geochemical thermometry have been proposed with the purpose to evaluate the original temperature, crystallinity and liquid composition for intrusive magmas at an initial stage corresponding to their emplacement into a magma chamber [*Ariskin and Barmina,* 2000]. Here the technique is applied to the Layered Series cumulates from of the Skaergaard intrusion.

A dataset of 65 bulk-rock compositions from the LZa ($n = 8$), LZb (16), LZc (11), MZ (20), UZa (10) units have been selected to use in geochemical thermometry. The structural location and chemical characteristics of the samples are listed in Table 1 of *McBirney* [1998]. The only change is in the sample LB-238 moved from LZb to LZa. In addition, five average bulk-rock compositions of the principal units of the Layered Series and five average compositions of equivalent rocks of the Marginal Border Series were used (Table 2).

3.1. Testing Closed System Calculations for the LZc Rocks

As was shown in the previous paragraph, the calculations for a system closed to O_2 seem to be more suitable if one tries to reproduce both the naturally observed modal mineral proportions and corresponding differentiated melt compositions. To conduct the closed system calculations for the Skaergaard rocks, I decided to use the bulk-rock FeO and Fe_2O_3 contents as a starting point for each of the above selected samples. This decision is based on the premise that most of the Skaergaard rocks are remarkably fresh and show little if any secondary oxidation. It allows one to assume that the phase equilibria simulations with the initial FeO and Fe_2O_3 contents may result in the intrinsic magmatic $Fe^{3+}/(Fe^{3+}+Fe^{2+})$ ratios in the residual liquids, providing a means of estimating redox conditions during differentiation.

To make sure that such calculations realistically reproduce both the original melt-mineral proportions and the residual liquid compositions we first calculated phase relations for 11 of the LZc rocks for which modal mineral proportions were available, see Table 3 of *McBirney* [1998]. Part of these data including those for Ilm and Mt is listed in Table 4. This tabulation also includes initial TiO_2, FeO and Fe_2O_3 contents in the LZc rocks with the normative proportions of the oxides calculated on the assumption that Ilm and Mt are pure end-members ($FeTiO_3$ and Fe_3O_4).

Results of phase equilibria calculations for the same LZc rocks are given in Table 4 in the form of modelled modal proportions at given amounts of crystallinity and chemical compositions (TiO_2, FeO, Fe_2O_3) of the complementary residual liquids for each sample. The calculations for conditions of closed O_2 were carried out at total pressure $P = 1$ kbar and an assumed H_2O content of 0.1 wt.% in all rocks. The results permit one to calculate total proportions of Fe-Ti oxides in the "computer simulated rocks" by summation

of the liquidus mineral proportions at a given system crystallinity with the normative oxide proportion in the residual liquid weighted in accordance with the modal amount of this melt. These estimates are given in two lower strings of Table 4. Comparisons with the observed modal proportions indicate that COMAGMAT-3.65 closely reproduces the final amounts of ilmenite and Ti-magnetite for all but two samples, LC-417 and LC-465.

3.2. Estimated LZa Characterstics

Using compositions of eight LZa rocks to estimate starting liquids, we have calculated the course of equilibrium crystallization up to a total crystallinity of 75 to 85%. These calculations were conducted at the same conditions as for the LZc rocks, with crystal increments $\Delta\sigma = 1$ mole %. For 5 of the initial compositions with MgO>9.5 wt.% (LA-36, -95, -237, -401, -770) a wider temperature range was obtained for Ol, and Pl was the second mineral to crystallize, followed by Aug and in some cases Mt, and finally by Pig: Ol (1322 to 1258°C) $\rightarrow$ Pl (1237 to 1193°C) $\rightarrow$ $Aug \pm Mt$ (1140 to 1110°C) $\rightarrow$ Pig (1125 to 1110°C). Relatively early crystallization of plagioclase and pyroxene was observed for the most calcium-rich sample, LA-238: Pl (1230°C) $\rightarrow$ Ol (1196°C) $\rightarrow$ Aug (1181°C) $\rightarrow$ $Mt + Pig$ (1120–1110°C), whereas the most silica-rich sample, LA-753 (51 wt.% SiO_2) indicated sub-cotectic relations: $Ol + Pl$ (1210 to 1200°C) $\rightarrow$ Aug (1153°C) $\rightarrow$ $Mt + Pig$ (1125 to 1115°C). Ilm was found in minor amounts in three cases at the temperatures <1110°C. Only in the most titanium- and iron-rich sample, LA-347, (5.8% TiO_2 and 18.3% FeO*) was Mt the first mineral to crystallize at 1190°C followed with Pl (1140°C), pyroxenes and ilmenite at 1120–1110°C.

Liquid lines of descent. Modelled trajectories of the residual liquid evolution are shown in the temperature-composition coordinates in Figure 8. For comparison, the average "LZa rock trajectory" calculated at QFM (Figure 5) has been added to these plots. One can see, that, with the exception of two samples, LA-347 and LA-753, (which were excluded from further consideration), the LZa liquid lines converge on an intersection in the range of 1140 to 1150°C. This is consistent with the premise that the other six LZa rocks could be interpreted as mechanical mixtures of Ol and Pl crystals plus a residual (interstitial) liquid. The average melt composition for this cluster of six converging lines at 1145°C is given in Table 3 and shown in Figure 8. Also shown is the composition of the equivalent unit of the Marginal Border Series calculated earlier at 1165°C ([*Ariskin,* 1999]; see TM composition in Table 1).

Initial mineral compositions. Calculated average compositions of Ol and Pl for the six samples at 1145°C are $Fo_{74.9\pm1.5}$ and $An_{66.3\pm1.9}$. The estimated An content in plagioclase is in excellent agreement with observed compositions (Figure 3), whereas the calculated Ol composition is 7 mole % more magnesian. This difference cannot be attributed to uncertainties of the COMAGMAT model, which generally has an accuracy of about 1–2% Fo [*Ariskin and Barmina,* 2000]. It is more likely to indicate re-equilibration

Table 4. Comparison of the modal proportions of Fe-Ti oxides observed in the LZc rocks of the Layered Series with those calculated by COMAGMAT at closed to oxygen conditions

Sample	LC-67	LC-306	LC-342	LC-406	LC-417	LC-465	LC-534	LC-605	LC-727	LC-746	LC-928
	Petrological observations										
	Bulk-rock compositions, wt.%										
TiO_2	4.82	4.51	12.84	6.71	3.48	9.89	0.98	2.96	9.52	9.43	6.55
FeO	15.56	16.45	20.34	12.30	12.25	17.03	11.10	10.78	18.67	16.27	11.99
Fe_2O_3	5.63	7.80	10.31	4.80	3.67	10.71	1.41	4.21	11.46	5.23	6.94
	Normative proportions of Fe-Ti oxides, wt.%										
Ilm	8.58	24.40	12.77	6.62	18.81	1.86	5.63	18.10	17.93	0.26	14.83
Mt	11.33	14.96	6.97	5.33	15.55	2.05	6.11	16.63	7.59	12.48	13.25
	Modal proportions of Fe-Ti oxides, wt.%										
Ilm	**4.5**	**3.9**	**23.1**	**12.7**	**8.0**	**16.8**	**0.9**	**3.5**	**13.0**	**14.9**	**11.1**
Mt	**13.5**	**14.5**	**8.2**	**4.0**	**2.1**	**5.6**	**2.2**	**5.2**	**23.7**	**9.8**	**10.1**
	Results of calculations in closed to oxygen systems										
	Modal proportions, wt.%										
% cryst	76.3	84.4	51.3	77.1	76.3	82.0	76.1	81.0	84.7	82.9	78.9
Ilm	2.6	3.5	21.2	9.5	0.6	17.2	0.0	1.4	14.5	11.7	9.2
Mt	12.3	15.3	8.9	7.0	8.6	17.2	1.0	6.7	21.9	11.6	9.9
Melt	23.7	15.6	48.7	22.9	23.7	18.0	23.9	19.0	15.3	17.1	21.1
	Residual melt compositions, wt.%										
TiO_2	4.27	3.94	3.76	3.95	3.16	2.60	2.63	3.02	2.40	4.76	3.79
FeO	14.32	12.35	13.59	13.42	11.17	7.22	13.07	8.14	6.03	15.08	10.32
Fe_2O_3	3.10	3.26	4.62	2.76	2.54	2.43	3.86	3.57	2.31	2.37	3.83
	Normative proportions of Fe-Ti oxides in the residual melts, wt.%										
Ilm	8.11	7.48	7.14	7.50	6.00	4.94	4.99	5.74	4.56	9.04	7.20
Mt	4.49	4.73	6.70	4.00	3.68	3.52	5.60	5.18	3.35	3.44	5.55
	Bulk proportions of Fe-Ti oxides in the modeled rocks (modal+normative), wt.%										
Ilm	**4.5**	**4.7**	**24.7**	**11.2**	**2.0**	**18.1**	**1.2**	**2.5**	**15.2**	**13.3**	**10.7**
Mt	**13.4**	**16.0**	**12.2**	**7.9**	**9.5**	**17.8**	**2.3**	**7.7**	**22.4**	**12.2**	**11.1**

Note: Normative proportions of the oxides were calculated on the assumption that *Ilm* and *Mt* are pure end-members (CIPW). The modal proportions were calculated by the regression technique of *Albarede and Provost* [1977] using the bulk-rock compositions and microprobe analyses of the observed minerals. Bulk proportions of Fe-Ti oxides in the modeled rocks were obtained by the summation of the modal mineral proportion calculated at a given system crystallinity with the normative proportion of oxides in the residual liquid weighted in accordance with the amount of the melt.

of the initial olivine crystals with an iron-enriched residual liquid constituting on average up to 50 wt.% of the mineral-melt assemblages (see below).

Oxygen fugacity. Also shown in Figure 8 are the $T - \log fO_2$ dependencies calculated for each liquid line of descent as a function of the evolving Fe^{3+}/Fe^{2+} ratio in the melt. These calculations use the equation by *Sack et al.* [1980] rearranged to compute $\log fO_2$ for a given temperature and melt composition. As was shown by *Nikolaev et al.* [1996], such calculations have an accuracy of ± 1 log unit. In ideally closed systems, the modelled $T - \log fO_2$ trajectories should intersect at the same temperature as the liquid compositions. In such a case, an average fO_2 value calcu-

lated for different evolutionary lines could be considered as an estimate of the oxygen fugacity intrinsic to the initial mineral-melt equilibrium assemblage. For the LZa molten rocks these lines form a wide cluster of $\log fO_2$ values (Figure 8) with an average of -7.5 ± 0.6 at $1145°C$. This is about 1.5 log units above the QFM buffer and is consistent with the measurements of *Kersting et al.* [1989]. Note that the standard deviations of 0.6 log units can be attributed to both the accuracy of Sack's equation and to the analytical uncertainties in the bulk-rock FeO and Fe_2O_3 contents. There is no reason to suspect that the COMAGMAT mass-balance calculations for the $Ol + Pl$ field are incorrect [*Yang et al.,* 1996].
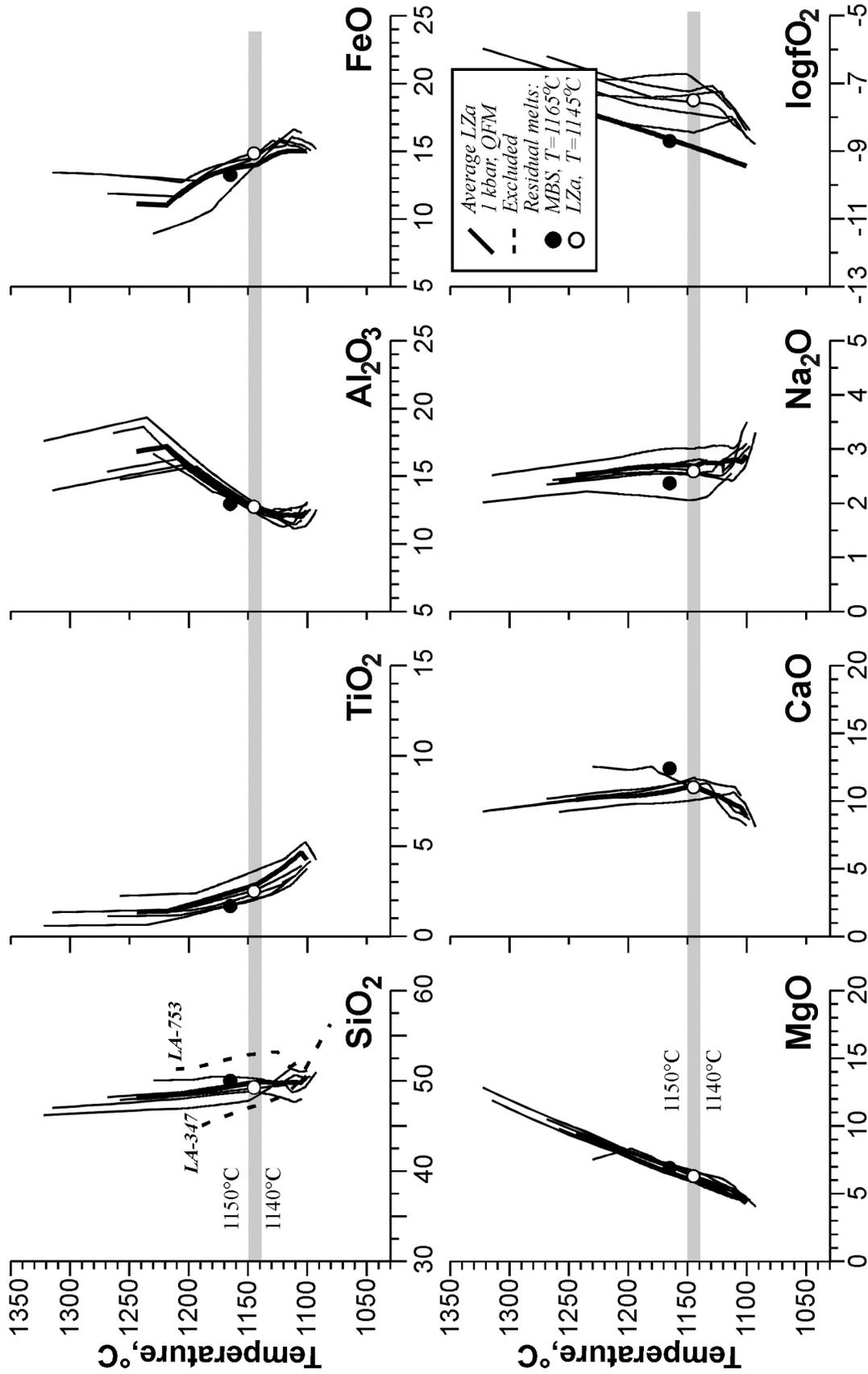
Figure 8. Results of geochemical thermometry for the LZa rocks at $P=1$ kbar and 0.1 wt.% H_2O in the starting compositions. Thin lines correspond to the equilibrium crystallization trajectories calculated at closed O_2 conditions for six Ol-Pl gabbros. The temperature of $1145\pm5°C$ is assumed to indicate that intrinsic to the residual liquid (Table 3). Thick line represents calculations for the average LZa composition at QFM (see Figure 5). Two dashed lines belong to the samples LA-347 and LA-753 are excluded from further considerations.
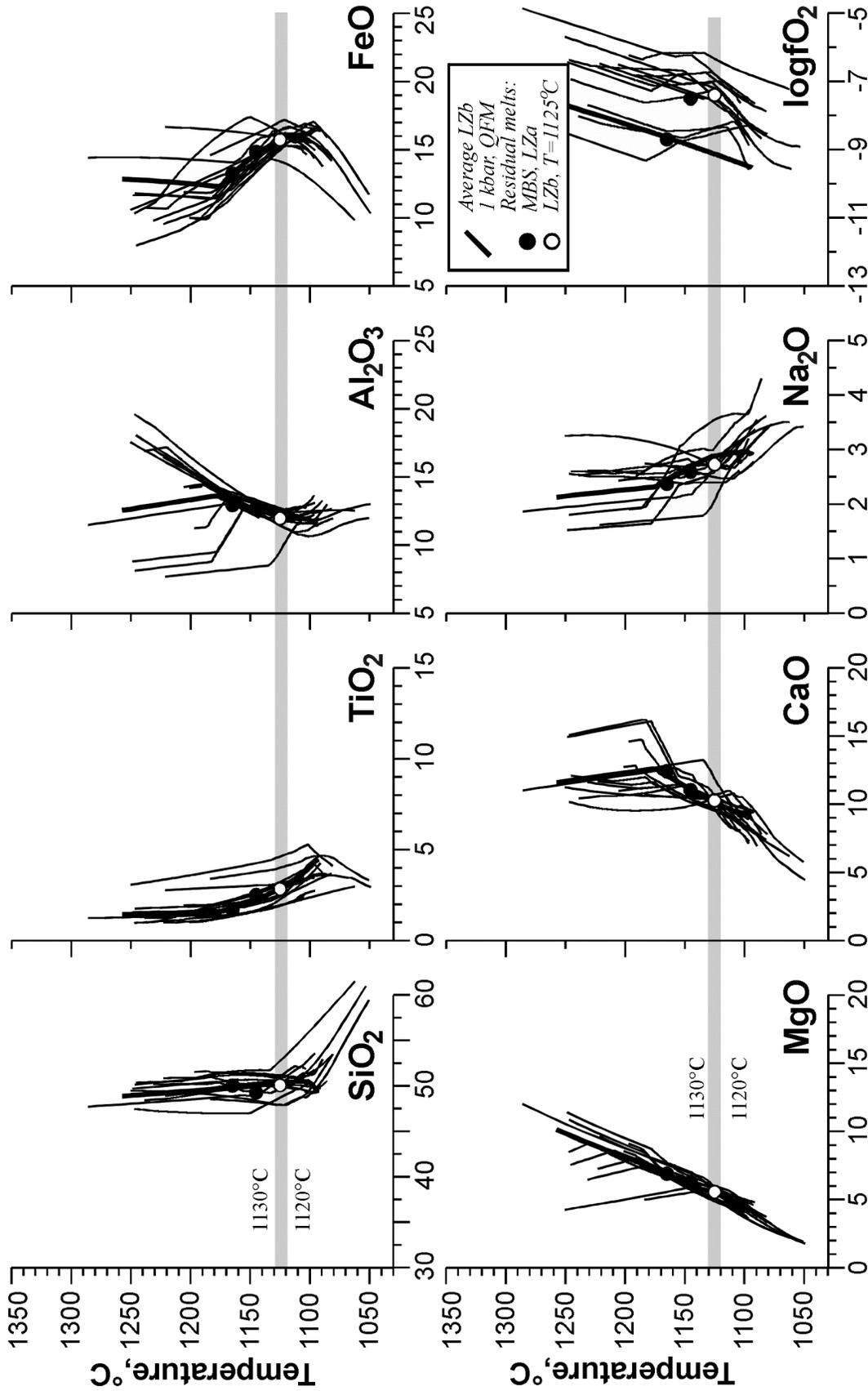
Figure 9. Results of geochemical thermometry for the LZb rocks at $P=1$ kbar and 0.1 wt.% H_2O in the starting compositions. Thin lines correspond to the equilibrium crystallization trajectories calculated at closed O_2 conditions for fourteen *Ol-Pl-Aug* gabbros. The temperature of $1125\pm5°C$ is assumed to be that intrinsic to the residual liquid (Table 3). Thick line represents calculations for the average LZb composition at *QFM* (see Figure 5).
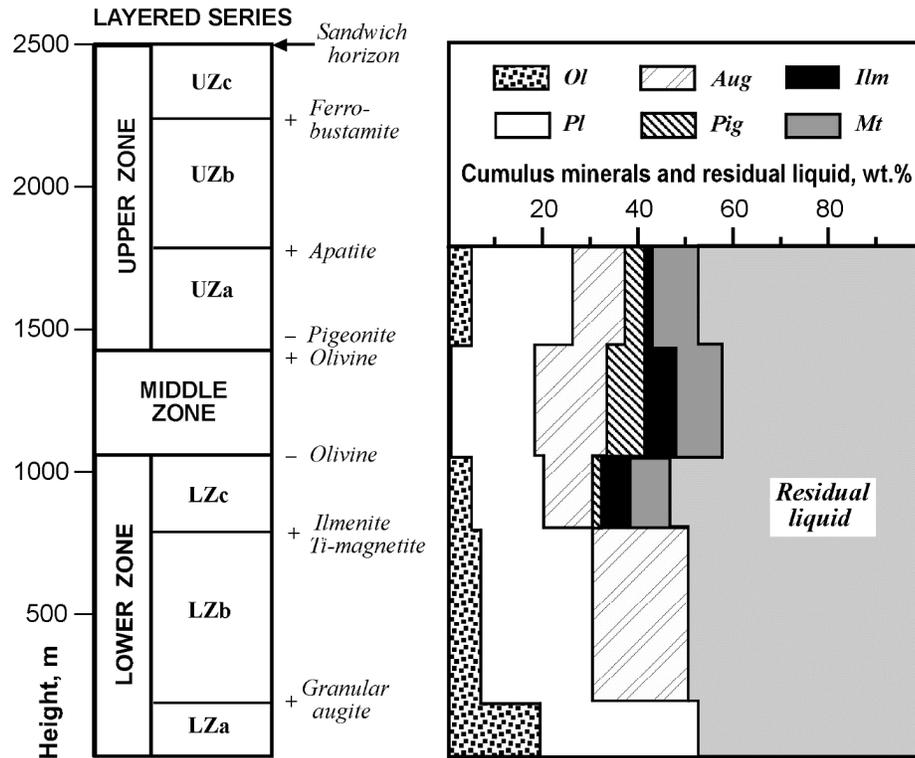
Figure 10. Calculated mineral-melt mixtures from which the rocks constituting the principal units of the Layered series formed. These modal proportions were estimated as an average of the amounts of different liquidus minerals and residual liquid equilibrated for each sample numerically at the formation temperatures intrinsic to five groups from the main LS zones (Table 3).

3.3. Estimated LZb Characteristics

Three main crystallization sequences were found to be peculiar to the LZb rocks. Four trajectories (LB-104, 234, 600, and 724) indicate the order: Ol (1370 to 1240°C) $\rightarrow$ Pl (1220 to 1170°C) $\rightarrow$ $Aug \pm Mt$ (1160 to 1110°C) $\rightarrow$ Pig (below 1130°C); in five cases (LB-68, 235, 269, 476, 655) augite appeared on the liquidus at temperatures of 1200 to 1170°C simultaneously with or just after olivine, and in all seven samples plagioclase was the first crystallizing mineral (1250 to 1190°C) followed by Ol and Aug. These phase relations indicate that Ol and Pl continued to be the main cotectic phases with Ca-rich pyroxene crystallizing as the third mineral. Ti-magnetite usually is the fourth, whereas Pig and Ilm were found only at late stages at temperatures below $\sim$1120°C and 1100°C, respectively. These calculations are in general agreement with petrological data indicating the change in the structural position and abundance of augite within the LZb horizon and do not contradict with a standard interpretation that Aug crystallized on a cotectic line with Ol and Pl [McBirney, 1989; Wager and Brown, 1967].

Liquid lines of descent constitute of a single family of cotectics converging at temperatures below 1140°C (Figure 9, two samples excluded). The most compact cluster of liquid compositions corresponds visually to 1125±5°C: this could

be accepted as the final equilibrium temperature at which melt was entrapped or ceased to infiltrate. The average liquid composition calculated for the LZb rocks at 1125°C (Table 3) is shown in Figure 9 along with compositions of TM (MBS) and LZa. The liquid follows the same trend of evolution charactered by an increase of FeO* at approximately constant silica contents.

Mineral compositions corresponding to the original equilibrium "frozen" into LZb bulk-rock compositions are given in Table 3. The modelled primary plagioclase ($An_{61.9\pm2.1}$) is slightly more calcic than the observed composition (Figure 3) but is within the accuracy of the geothermometers used for Pl-melt [Ariskin, 1999]. Olivine ($Fo_{72.1\pm2.1}$) becomes more ferrous than in LZa rocks. These deviations clearly correlate with the decrease in the amount of modal Ol crystals in LZb rocks (Figure 10) and with the iron enrichment of the residual liquid. It offers indirect evidence of re-equilibration with liquids expelled from lower levels of the Layered Series. Modelled augites (Table 3) are also more magnesian than natural pyroxenes, although these differences are not large (Figure 3). Again, this is consistent with earlier observations indicating insignificant of Cpx re-equilibration in differentiated intrusions [Barmina et al., 1989a]. Average proportions of interstitial material are estimated at 50±10 wt.%. The oxygen fugacity was calculated to be similar to that of the LZa rocks with an average log fO_2 of -7.4 ± 0.7.
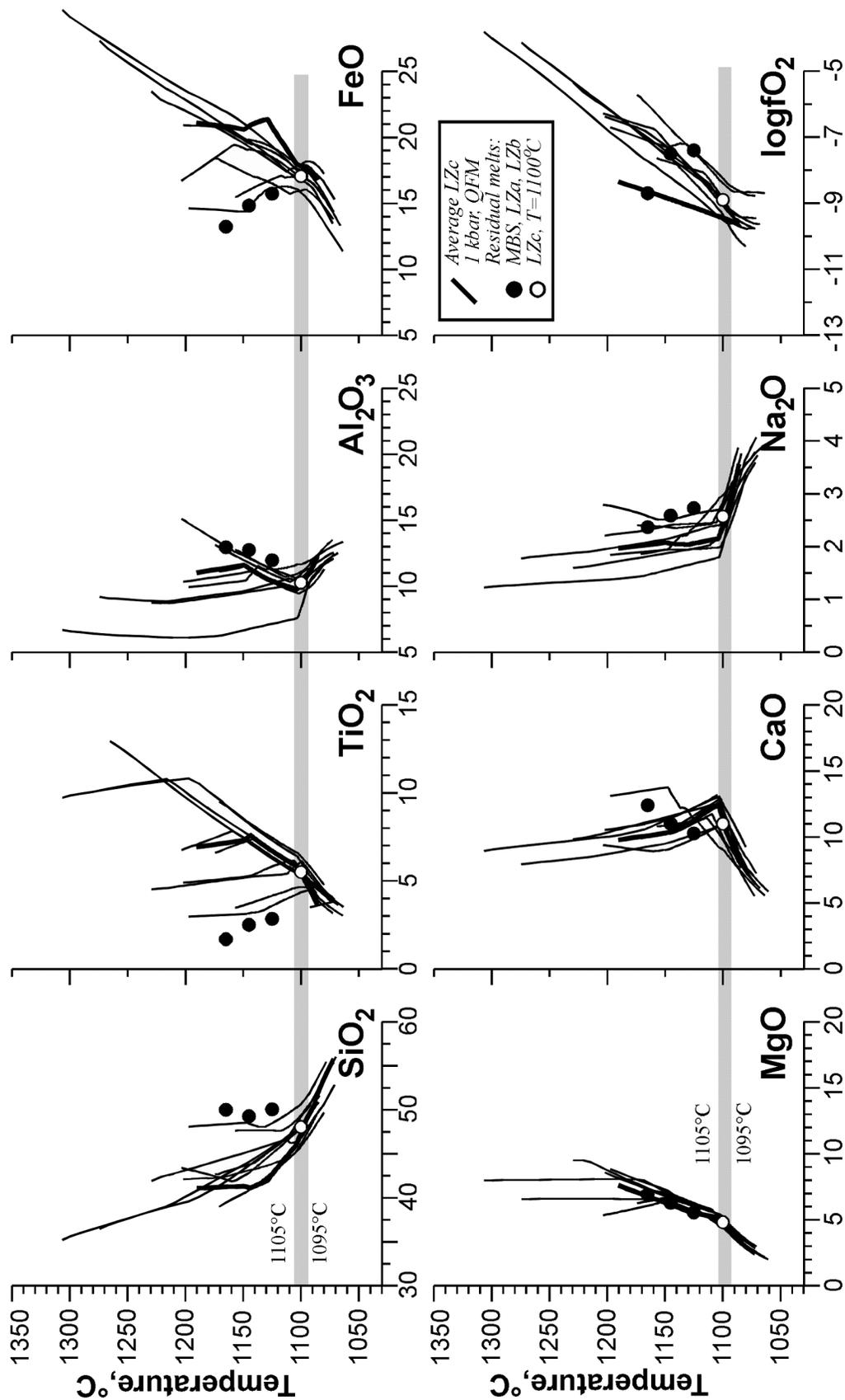
Figure 11. Results of geochemical thermometry for the LZc rocks at $P=1$ kbar and 0.1 wt.% H_2O in the starting compositions. Thin lines correspond to the equilibrium crystallization trajectories calculated at closed O_2 conditions for nine Ol-Pl-Aug-Mt-Ilm ± Pig gabbros. The temperature of $1100\pm5°C$ is assumed to be that intrinsic to the residual liquid (Table 3). Thick line represents calculations for the average LZc composition at QFM (see Figure 5).

3.4. Estimated LZc Characteristics

Compared to LZa and LZb, simulations for eleven LZc compositions show much more diversity in the order of appearance of minerals on the liquidus. This is due to the abundant crystallization of oxides, so that for 6 samples (LC-306, 342, 465, 727, 746, and 928) Ilm and Mt are the first minerals to crystallize in the range of 1270 to 1170°C. The order of crystallization of silicate minerals for these samples is variable ($Ol \to Pl \to Aug+Pig$ or $Ol \to Aug+Pig \to Pl$), however pyroxenes never crystallized at temperatures above 1110°C. This can be taken as the upper limit for the temperature controlling original mineral-melt equilibria. In three cases Ol crystallized first (LC-67, 534, and 605) followed by Pl, pyroxenes and oxides. Sample LC-406 indicated over-saturation with plagioclase (1203°C), whereas LC-417 started with the cotectic assemblage $Ol+Pl$ (1157°C). These results support the notion that Ilm and Mt should be considered among the major primary phases of LZc [*Wager and Brown,* 1967].

Liquid lines of descent for the LZc rock melts are shown in Figure 11. They have excellent intersections of the calculated trajectories near 1100°C (two samples LC-342 and LC-534 were excluded). As compared to the modelled melt for LZb, the average LZc liquid at 1100°C is slightly poorer in SiO_2 and markedly richer in TiO_2 and FeO^* (Table 3). Both alumina and magnesia continue to decrease, whereas a small increase in CaO is observed in the LZc residual liquids (Figure 11). The relative CaO enrichment is difficult to interpret in terms of crystal fractionation models involving simultaneous precipitation of Pl and high-Ca pyroxene. Note, however, the increase in calcium is certainly within the accuracy of the technique, as indicated by the 1σ deviations for the CaO contents in the LZb and LZc liquids (Table 3).

Mineral compositions of Ol, Pl, and pyroxenes equilibrated with the LZc residual liquid have the same tendency to have low amounts of the refractory components compared to the underlying mineral-melt assemblages (Table 3). Appearance of Pig crystallizing near 1100°C was observed only five times of the 11 samples, so that the question of its original primary nature in the LZc rocks is still open to question. The initial Ilm and Mt compositions are given in Table 3 in the form of the $FeTiO_3$ and Fe_2TiO_4 activities calculated using the equations of *Stormer* [1983]. These data indicate almost stoichiometric ilmenite and moderately titaniferous magnetite. This is consistent with a shift of the calculated fO_2 values towards more reduced conditions close to the QFM buffer (Figure 11).

3.5. Estimated MZ Characteristics

Twenty of the MZ samples analysed by *McBirney* [1998] were used in the phase equilibria calculations. Differences in the starting compositions and the extent of iron oxidation result in various crystallization sequences in which six minerals ($Ol, Pl, Aug, Pig, Ilm, Mt$) change or replace each other over small temperature intervals, often within the accuracy of the COMAGMAT model (10–15°C). Only their general

features are described here. The most surprising result is that all Ol-free samples produce some amount of olivine at early and middle stages of crystallization. On average, the amount of olivine was 3 to 5 wt.% at 30% total crystallinity, but in some cases it was as much as 8 to 10 wt.% Ol. In eight samples Ol was the first mineral to crystallize at temperatures of 1190 to 1160°C (MZ-53, 55, 58, 61, 747, 824, 826, 831). However, at lower temperatures corresponding 50 to 70% crystals this olivine was completely dissolved by reaction with pyroxenes, oxides and melt. For the eight samples that contain the most TiO_2 and iron (MZ-28, 172, 438, 603, 613, 729, 830, 901), Fe-Ti oxides crystallized first, followed by Ol, Pl, and pyroxenes. In four cases, the starting melts were slightly oversaturated with plagioclase at 1210 to 1160°C (MZ-99, 343, 530, 864). Note that in only two cases was Aug found at temperatures above 1105°C, whereas Pig always crystallized below 1100°C. It is important to note that in half of the samples pigeonite appeared at a total crystallinity of 20 to 40%. This may indicate that the mineral may have been among the primary crystallizing phases. In any case, a substantial amount of Pig was certainly formed at later stages by the peritectic replacement of olivine.

Liquid lines of descent calculated for seventeen MZ rocks had remarkably uniform convergence toward an intersection at temperatures below 1100°C (Figure 12). Three samples, MZ-172, 613, and 830, gave less consistent results. That this was true despite the different modelled crystallization sequences makes one confident that the bulk-rock chemical compositions of these MZ rocks really preserve a record of their original phase equilibria and the composition of their residual liquid. This situation, however, poses a problem in identifying the equilibrium temperature, because the calculated trajectories are almost parallel after their intersection slightly below 1100°C. In principle, it is possible to use the natural Pl composition at the base of the Middle Zone ($\sim An_{51}$, Figure 3) as a criterion for the average temperature for the 17 evolutionary lines. However, at this stage I assume a higher temperature of 1090°C as an upper limit for the estimate. The average residual liquid composition calculated at 1090°C is given in Table 3 and illustrated in Figure 12. Compared to the underlying LZc assemblages, the MZ residual liquid is slightly richer in silica, iron, and alkalies with a complementary decrease in TiO_2, MgO and CaO; the Al_2O_3 content is the same. Note that the titanium depletion is caused by precipitation of ilmenite and magnetite in approximately equal amounts (Figure 10). The small iron enrichment is consistent with results of the simulations in systems closed to oxygen (Figure 7).

Mineral compositions in Table 3 are weighted average values for Ol, Pl, pyroxenes and oxides at 1090°C. The modelled Pl composition ($An_{54.2\pm2.9}$) is close to the observed plagioclase composition of An_{51}, while calculated pyroxenes and olivine relicts are again more magnesian. Ilmenite became slightly richer in $FeTiO_3$, whereas the activity of the ulvospinel component in Ti-magnetite increased considerably (Ulv_{72} in MZ versus Ulv_{54} in LZc). At first view this seems strange, because the calculated TiO_2 in the melt was found to decrease somewhat. However, if one considers the $T - \log fO_2$ diagram (Figure 12), it is clear that within the MZ zone the system was evolving to more reduced condi-
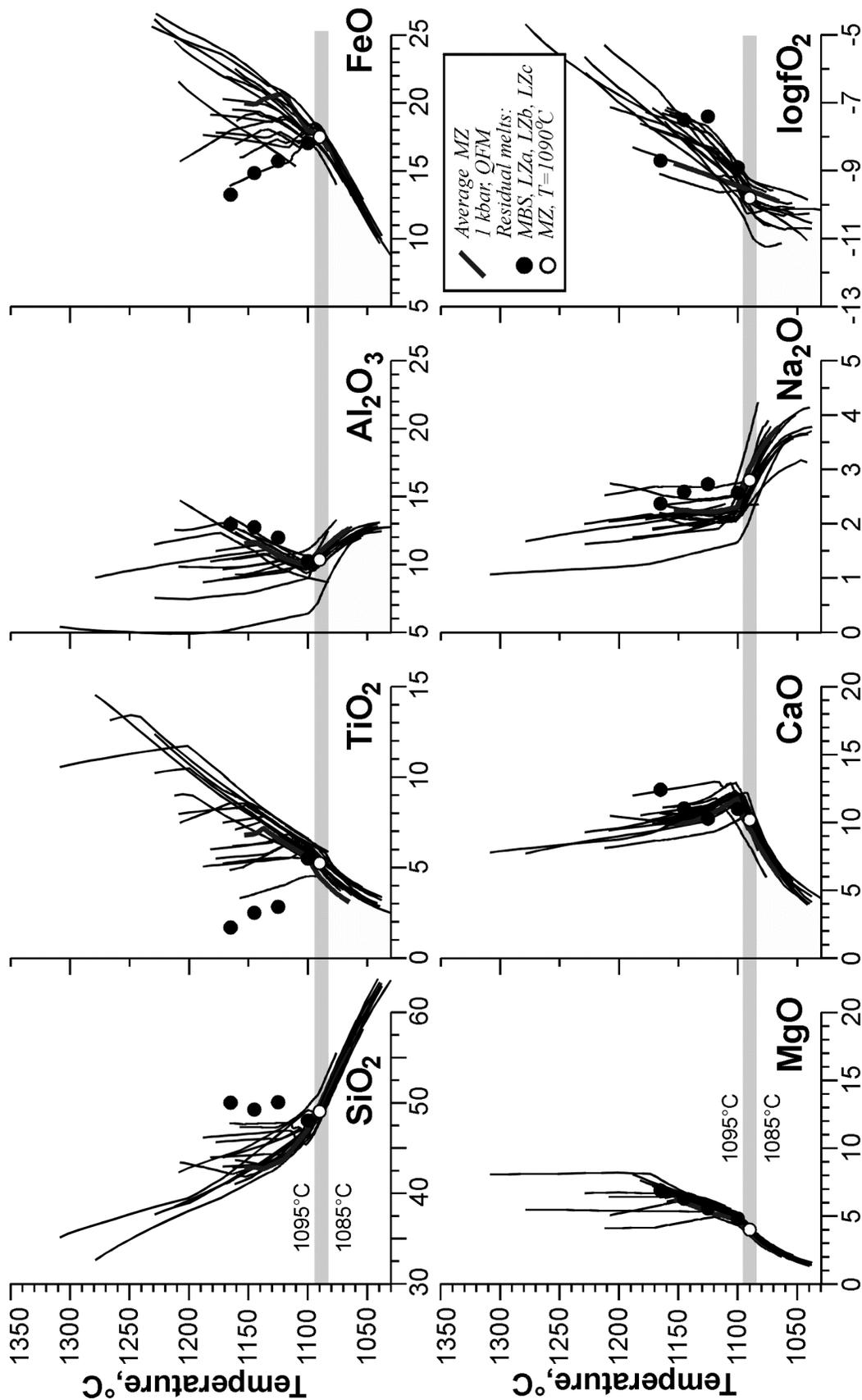
Figure 12. Results of geochemical thermometry for the MZ rocks at $P=1$ kbar and 0.1 wt.% H_2O in the starting compositions. Thin lines correspond to the equilibrium crystallization trajectories calculated at closed O_2 conditions for seventeen Pl-Aug-Mt-Ilm-$Pig \pm Ol$ gabbros. The temperature of $1090 \pm 5°C$ is assumed to indicate that intrinsic to the residual liquid (Table 3). Thick line represents calculations for the average MZ composition at QFM (see Figure 5).

tions, slightly below QFM (Table 3). This conclusion is in excellent agreement with the previous thermodynamic and experimental estimates indicating a smooth fO_2 decline towards MZ, where redox conditions corresponded to about 0.5 log units below QFM [*Frost and Lindsley,* 1992; *McBirney,* 1996; *Morse et al.,* 1980; *Williams,* 1971]. On the other hand, this somewhat surprising behavior may indicate that the initial Fe_2O_3 and FeO contents used in the closed system calculations really reflect both the total amount of oxides and Fe^{3+}/Fe^{2+} ratios intrinsic to the MZ residual liquids. It supports the premise that most of the Skaergaard rocks have undergone insignificant secondary oxidation.

3.6. Estimated UZa Chacteristics

Phase equilibria calculations for ten LZa rocks produced the lowest temperatures for those parts of the Layered Series studied thus far. None of the assemblages had a silicate liquidus temperature above 1180°C. On average, the modelled sequences are similar to those of MZ (Figure 5), starting from sub-cotectic ($Ol + Pl\pm$ oxide) or compositions slightly oversaturated with olivine (UA-102, 136, 199, 200, 300, 315, 614, 786). The two samples with the highest FeO contents (UA-131 with 35 wt.% and UA-425 with 46 wt.%) have a large magnetite field and were excluded from further considerations because of strong deviations of their trends from those calculated for other samples. Both pyroxenes crystallized almost simultaneously at temperatures below 1100°C, with the Pig crystallization interval slightly decreased with respect to the MZ simulations. This resulted in an increase in the modal proportion of Ol (Figure 10), but Pig did not disappear completely (as can be seen in Figure 3) but continued to be a primary phase. This corresponds observations of nature that Pig continued continued to present in many rocks in the lower half of UZa [*McBirney,* pers. comm.].

Liquid lines of descent for the UZa rocks resemble those of MZ with a cluster of residual liquid compositions in the range of 1090 to 1080°C (Figure 13). The average calculated liquid composition at 1085°C is characterized by minor silica enrichment and total iron that is practically the same as in the MZ liquid (Table 3). In general, the UZa residual melt maybe considered the fractionated liquid with the lowest MgO and CaO contents and highest alkalinity. A small decrease in P_2O_5 is considered to be within the accuracy of the geochemical thermometry (Table 3). The moderate phosphorus concentrations could certainly have evolved from the low P_2O_5 contents in the MZ and UZa rocks, which rarely exceed 0.1 wt.% [*McBirney,* 1998]. However, it should be noted that the appearance of primary apatite in UZb implies that at that level the liquid must have contained at least 0.8 to 1.2 wt.% P_2O_5 [*Toplis et al.,* 1994].

Mineral compositions of the six-phase liquidus assemblage calculated at 1085°C follow the same trend of the depletion in the refractory components as in lower horizons (Table 3). The modelled plagioclase ($An_{48.0\pm3.1}$) is similar to the composition of An_{46} observed at the base of UZa (Figure 3), whereas the calculated Ol ($Fo_{52.5\pm2.5}$) is much more magnesian than the observed composition (Fo_{40}). Both

pyroxenes have higher Fs/En ratios, although the modelled augite is of 4 to 5 mole % richer in Wo than the natural one. Although the ilmenite composition remains unchanged, magnetite demonstrates a further increase in Fe_2TiO_4 (81.4±6.7 mole % Ulv).

4. Discussion

Geochemical thermometry for the Layered Series rocks produced a probable range of the "formation temperatures" that represent original interstitial material (Table 3). It spans a range of only 60°C between 1145±10°C at LZa to 1085±10°C at UZa. The observed values correspond to other estimates based on other approaches [*Hoover,* 1989; *Jang and Naslund,* 2001; *McBirney and Naslund,* 1990; *Williams,* 1971]. The phase equilibria simulations also define the range of oxygen fugacities intrinsic to the initial liquids. Our results indicate a sharp decline in $\log fO_2$ values from 1 to 1.5 units above QFM in LZa and LZb to QFM and lower oxygen fugacities starting from LZc. This is also in fairly good agreement with previous estimates [*Frost and Lindsley,* 1992; *Frost et al.,* 1988; *Kersting et al.,* 1989; *Lindsley et al.,* 1969; *Morse et al.,* 1980; *Williams,* 1971].

The main result of the geochemical thermometry is an estimate of the initial compositions of differentiated liquids (Table 3). The calculated liquids demonstrate strong enrichment in FeO (up to ∼18 wt.%) and TiO_2 (up to ∼5.5 wt.%), consistent with the notion that the Skaergaard magma evolved in a manner typical of iron- and titanium-rich tholeiitic magmas [*Brooks et al.,* 1991]. As *Wager and Brown* [1967] inferred from simple mass-balance considerations, there was essentially no silica depletion in the liquids from LZa through UZa. Phase equilibria calculations do, however, indicate a small increase in SiO_2 during formation of LZa. This agrees with the results of melting experiments for Ol-Pl assemblages in low-pressure tholeiitic systems [*Grove and Baker,* 1984]. The transition from the LZb ($Ol + Pl + Aug$) to LZc ($Ol + Pl + Aug +$ oxides) rocks is accompanied by a decrease in SiO_2 as a result of continued crystallization of Ca-rich pyroxene, whereas the appearance of Mt and Ilm brings renewed silica enrichment.

It is interesting that this increase in SiO_2 is not as significant as it commonly is during crystallization of Fe-Ti oxides from tholeiitic magmas buffered for fO_2 [*Ariskin and Barmina,* 1999, 2000]. It is certainly consistent with the absence or very small decrease in FeO (Table 3) that could be interpreted as evidence that the Skaergaard magma evolved as a system closed to oxygen [*Osborn,* 1959; *Presnall,* 1966; *Toplis and Carroll,* 1996]. Nevertheless, we draw attention to the fact that the decrease of fO_2 within this temperature range *is too sharp to be generated during simple closed-system crystallization.* It moves us to conclude that the Skaergaard magma chamber has not been absolutely closed and could have been open to a reducing agent that was responsible for the change of oxygen fugacity during a middle-to-late stage of differentiation.

Another important factor bearing on the trend of differentiation is the modal proportions of primary mineral as-
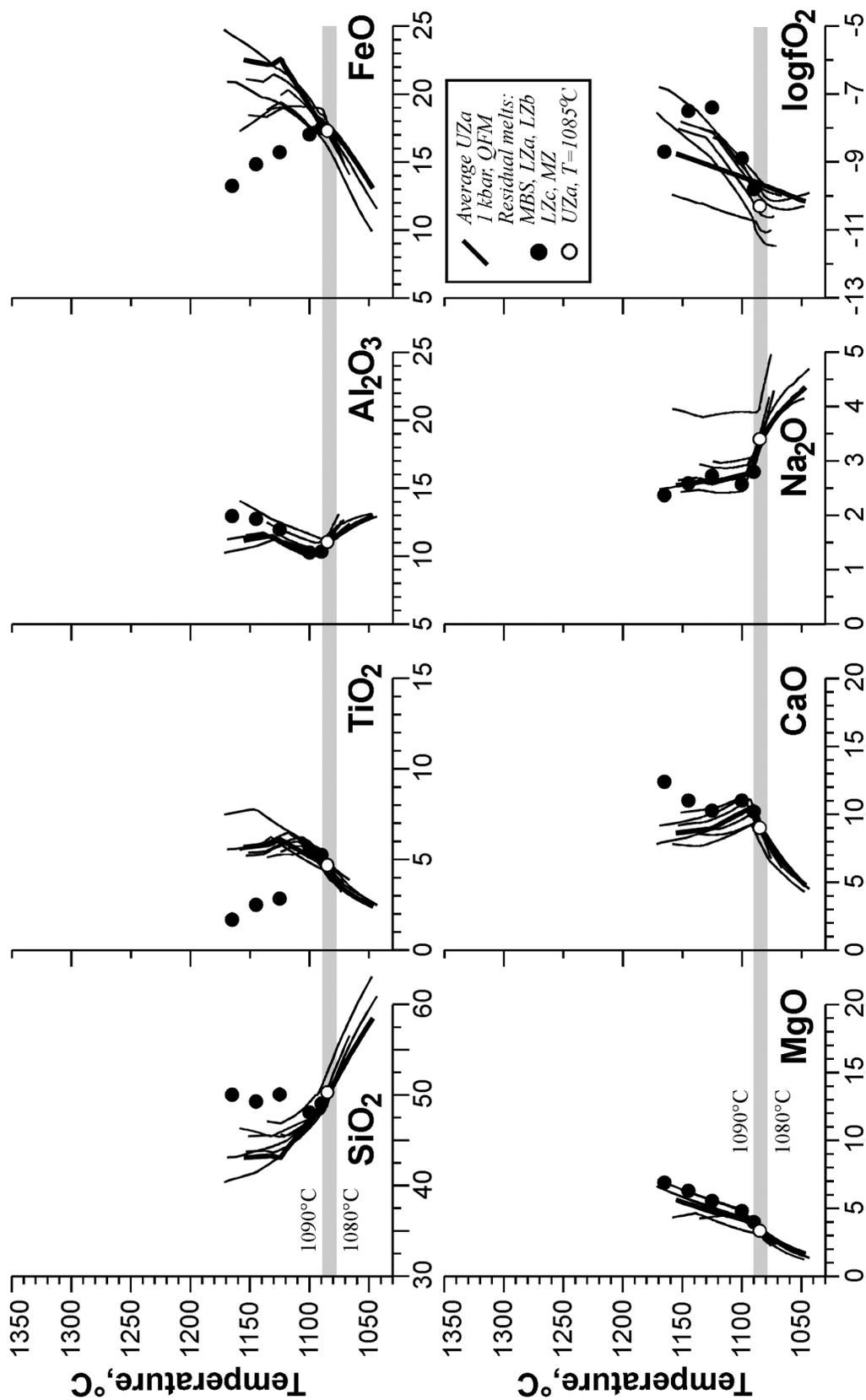
Figure 13. Results of geochemical thermometry for the UZa rocks at $P=1$ kbar and 0.1 wt.% H_2O in the starting compositions. Thin lines correspond to the equilibrium crystallization trajectories calculated at closed O_2 conditions for eight Pl-Aug-Mt-Ilm-Pig-Ol gabbros. The temperature of $1085 \pm 5°C$ is assumed to indicate that intrinsic to the residual liquid (Table 3). Thick line represents calculations for the average UZa composition at QFM (see Figure 5).

semblages and residual (interstitial) liquids. Figure 10 summarizes the results of the geochemical thermometry calculations related to the original characteristics. The diagram to the right of the figure was constructed from average modal proportions calculated for each unit at the corresponding temperature (Table 3). The observed modal assemblages closely resemble the major calculated proportions of minerals for the main Skaergaard units. The only exception is probably over-estimated amounts of pigeonite in the UZa zone, although the mineral is known to present in small amounts there [*McBirney,* 1989; 1996]. Similarly, the modelled proportions of the evolving residual liquid through the LS section considered here was found to be about 50 wt.% (Figure 10). This may indicate that the compaction process was not efficient, at least at the early and middle stages of the Skaergaard magma differentiation. This conclusion is consistent with petrographic observations that adcumulus textures (expected to indicate a higher crystallinity) were widely observed at higher levels corresponding to UZb and UZc horizons [*Wager and Brown,* 1967]. Note, however, that the modal-proportion diagram in Figure 10 represents average values for the main units: in fact, the calculated amounts of intercumulus liquid differ for each particular rock, ranging from about 30% to 60% (as a *residual porosity – Morse* [1981]).

4.1. Some Contradictions

The most conspicuous contradiction of the results of geochemical thermometry is the obvious gap between LZa and LZb liquids and those of LZc through UZa (Table 3). It is seen in a small (~1 wt.%) return of CaO contents to higher and SiO_2 contents to lower values starting from the LZc liquid (Figures 11–13). The simplest explanation would be that the differences are due to uncertainties of the COMAGMAT program, because the gap is within the accuracy of the technique (compare the 1σ deviations in Table 3). One could say that the COMAGMAT-3.65 model slightly under-estimates the crystallization temperature for *Aug* (Figure 5), so that later precipitation of the high-Ca pyroxene was modelled from more calcium rich liquids. Nevertheless, a nearly two-fold increase in TiO_2 from LZb to LZc must also be explained because it would require at least 40 to 50% crystallization of the LZb melt. Thus, the observed gap may be an important genetic clue that should be examined more closely.

The inconsistencies can be seen more clearly if the calculated TM (MBS, Table 1) and residual liquid compositions (Table 3) were plotted on the $OLIV$-CPX-QTZ diagram proposed for tholeiitic and calc-alkaline magma crystallizing systems (Figure 14). The generalized diagram has been constructed by processing a large dataset from 1 atm melting-experiments and is based on a projection scheme developed by Grove and his colleagues [*Grove,* 1993; *Grove and Baker,* 1984; *Tormey et al.,* 1987]. It includes low-pressure *Ol*-pyroxene boundaries corresponding to natural cotectic melts saturated with plagioclase. In addition to the modelled liquids, Figure 14 shows Wager's mass-balance compositions [*Wager,* 1960; *Wager and Brown,* 1967] and the partial melts of Layered Series rocks [*McBirney and Naslund,* 1990].
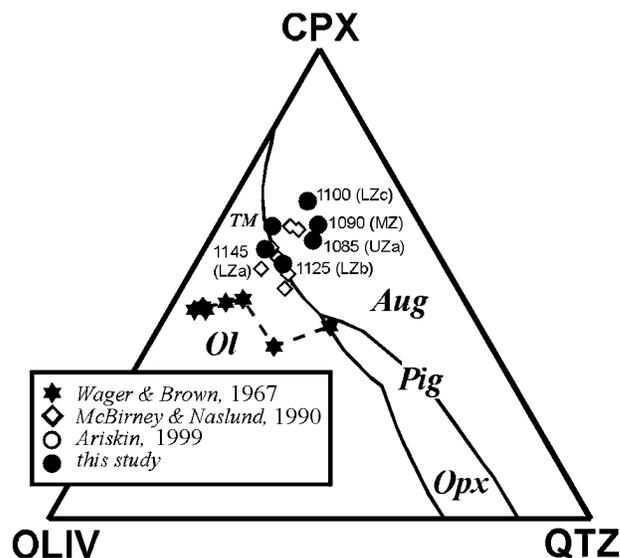
Figure 14. Liquidus compositions representing the trapped and residual liquids estimated by geochemical thermometry, experimentally obtained "trapped" melts [*McBirney and Naslund,* 1990], and the canonical series of the Skaergaard differentiates [*Wager,* 1960; *Wager and Brown,* 1967]. The modeled liquids include the average trapped melt defined for the MBS rocks (TM, Table 1) and five residual liquids for the main units of the Skaergaard Layered Series (Table 4). Liquids plotted on this diagram are plagioclase-saturated and outline the *Ol-Aug-Pl* and *Ol-Aug-Pig-Pl* saturation surfaces.

First of all, note that Wager's classical trend is totally inconsistent with the standard low-pressure evolution of crystallizing tholeiitic magmas. With one exception, these points lie in the *Ol-Pl* field far from the experimentally defined *Ol-Aug-Pl* boundary, even though most of points should correspond to co-saturation with olivine and Ca-rich pyroxene. Only the last point is found to fall in the *Ol-Pl-Aug-Pig* field, but this is not surprising because the composition is similar to that of the Sandwich Horizon which is thought to represent an almost pure liquid that was the final product of differentiation [*Wager and Brown,* 1967]. It allows us to conclude that the trend of FeO versus SiO_2 calculated using inferred proportions of the main differentiated units of the Skaergaard intrusion (Figure 1) is actually artificial and does not provide a valid interpretation of all the major components of tholeiitic magmas. The only way it can be made to correspond to experimental data is to assume crystallization at elevated pressures where the CPX field is increased. In such a case, one should re-examine the previous pressure estimates of *Lindsley et al.* [1969] and assume that *Aug* crystallized as a primary mineral beginning from the LZa zone.

The experimentally determined compositions of *McBirney and Naslund* [1990] and the calculated compositions of residual liquids of *Ariskin* [1999; this study] have a more realistic distribution in Figure 14. Most of the points are in

Table 5. Comparison of possible Skaergaard parental magmas with bulk intrusion compositions calculated from exposed rock types

Sample	Probable parental magmas (see Table 1)		The Skaergaard intrusion compositions (LS/UBS/MBS)		
	KT-39	TM (MBS)	50/20/30	40/40/20	40/20/40
SiO_2	50.46	49.94	46.26	47.55	46.11
TiO_2	2.70	1.68	4.22	3.90	4.12
Al_2O_3	13.41	12.93	12.40	12.78	12.47
FeO_{tot}	12.96	13.22	17.26	16.71	17.30
MnO	0.22	0.19	0.27	0.26	0.27
MgO	6.71	6.89	6.29	5.49	6.44
CaO	10.34	12.38	10.07	9.77	10.12
Na_2O	2.41	2.37	2.40	2.62	2.36
K_2O	0.57	0.26	0.36	0.47	0.36
P_2O_5	0.22	0.15	0.45	0.46	0.44

Note: Three estimates of the Skaergaard intrusion composition are average characteristics [*McBirney,* pers. comm.] weighted in accordance with assumed proportions between the main structural units, including the Layered Series (LS), the Upper Border Series (UBS), and the Marginal Border Series (MBS). All compositions are normalized to 100 wt.%.

the vicinity of the *Ol-Aug* boundary which spans a range of liquids in which the upper margin is shifted slightly towards *CPX*. This is consistent with the presence of augite as a primary liquidus mineral dominating the course of crystallization for the most of the Layered Series rocks. Note that the calculated *TM*, LZa, and LZb liquids are located very close to the curve with a trend directed straight towards the *Pig* field, whereas the LZc to UZa melts with more normative diopside are located above the *Ol-Aug-Pig* peritectic point. It is difficult to find a reasonable petrologic interpretation that can link the two slightly different series of residual liquids by simple crystal fractionation. The first one is most likely to reflect the early stages of differentiation along the normal trend of tholeiitic magmas as seen in volcanic suites [*Ariskin et al.,* 1988; *Hunter and Sparks,* 1987; *Toplis and Carroll,* 1996]. The second trend may represent another type of chemical evolution that has only recently been suspected. Possible explanations include the possibility that the diopside normative and Ti-rich component was (i) a late stage residual liquid percolating upward through compacting crystals, (ii) an influx of the titanium and chlorine rich fluid at a middle-to-late stage [*McBirney,* in press], or (iii) some sort of compositional stratification in the main mass of magma. I think that any of the proposed mechanisms is linked with a more general Skaergaard problem concerning the absence of the mass-balance between probable parental magmas and the average Skaergaard intrusion composition.

4.2. A Skaergaard Parent – Differentiates Misbalance Problem

If we assume the Skaergaard Layered Series was formed during a closed system process of crystal fractionation from a parental magma close in composition to the marginal gabbro or the calculated initial "trapped" melt (Table 1), one would expect the weighted average composition of the Layered Series and two Border Series to resemble that of the proposed parental magma. Because the original shape of the intrusion is unknown, it is very difficult to estimate reliable proportions between the LS, UBS, and MBS rocks. Nevertheless, there are reasons to consider the LS rock as constituting at least 40–50% of the intrusion rocks providing the main contribution to the whole-body composition [*McBirney,* pers. comm.].

The main feature of the Layered Series is the predominance of magnetite- and ilmenite-rich rocks that compose of about 70% of the observed section (Figure 10). These rocks contain of 43 to 44 wt.% SiO_2, 5 to 6 wt.% TiO_2, and 22 to 23 wt.% FeO*, so that the average Layered Series composition must also be depleted in silica. The LS characteristics used to calculate a range of possible Skaergaard intrusion average compositions ($SIAC$), using varied proportions of the UBS and MBS rocks. Some of the results for three different proportions of the LS, UBS, and MBS are listed in Table 5. For comparisons, two compositions representing the chilled gabbro KT-39 and our calculated initial "trapped" liquid (Table 1) are also included into the table. Even a superficial view of the compositions reveals a strong misbalance between the parental compositions and that of the differentiated body. It is most apparent for TiO_2 and P_2O_5 which are almost two fold higher in $SIAC$ as compared to the proposed parents. Moreover, the intrusion composition has of 2–4 wt.% less SiO_2 and much more iron. The observed discrepancy may be explained by the effects of closed- or open-system crystallization. The "closed" interpretation includes two possibilities, one in which the bulk composition of the Layered Series has more SiO_2 and less TiO_2, FeO, and phosphorus than the exposed section. This would imply a "Hidden Layered Series" with relatively silica-rich *Pl-Opx* rocks at depth [*Wager and Brown,* 1967]. The second possible explanation postulates substantial amounts of felsic differentiates almost completely removed by erosion [*Hunter and Sparks,* 1987].

Results of our calculations indicate that the compositional difference between liquids "trapped" in marginal rocks (TM)

and that of LZa is small (Tables 1 and 3, Figure 14). They are consistent with the observation that the composition of Pl at the base of the exposed Layered Series is similar to that in the uppermost part of the Upper Border Series (Figure 3). Thus, there are no reasons to assume a large volume of a "Hidden Layered Series", assuming, of course, that the initial Skaergaard magma was free of suspended crystals. If one suggests the Skaergaard magma came to the chamber with an amount of crystalline material $(Ol + Pl)$ equilibrated with a liquid close to the TM composition [*Ariskin,* 1999], the existence of complementary troctolitic rocks is inevitable, despite of some geophysical data arguing against the huge Hidden Zone [*Blank and Gettings,* 1973; *McBirney,* 1975]. Even if some amount of hidden troctolitic material exists, however, it is unlikely that crystallization in a closed system could produce large volumes of rocks rich in Fe-Ti oxides without more felsic differentiates (see Figure 7 and Figures 11–13).

In recent years more attention has been given to open-system crystal fractionation in the Skaergaard magma chamber with a later influx of a fluid or melt that was very rich in iron and titanium. There is some evidence of this in the geological relations, trace-element distribution, and petrographic features [*McBirney,* 1995]. Thus, this alternative interpretation may be also attractive in the light of the calculated shift of the LZc to UZa residual liquids plotted in the $OLIV$-CPX-QTZ diagram (Figure 14). Note, however, that a postulated influx of iron-rich material is difficult to reconcile with the vast amounts of the fluid needed to alter the primary igneous rocks metasomatically, or with the recent geochemical evidences for differentiation under closed conditions [*Jang and Naslund,* 2001].

5. Conclusions

A specially calibrated version of the COMAGMAT program allowed the author to define the range of initial temperatures (1145 to 1085°C) and oxygen fugacities (1–1.5 log units above QFM to slightly below QFM) intrinsic to the original crystal mush from which the rocks from LZa to UZa have been crystallized. In parallel, average major-element compositions of residual (interstitial) liquid were calculated for the same units (Table 3). The result demonstrates a trend of continual enrichment of FeO* (up to ∼18 wt.%) and TiO$_2$ (up to ∼5.5 wt.%) with only minor variations in the SiO$_2$ contents (48 to 50 wt.%).

Projection of the compositions onto the low-pressure $OLIV$-CPX-QTZ diagram (Figure 14) supports several lines of petrologic evidence that most of the Layered Series crystallized on an olivine-clinopyroxene cotectic (along with plagioclase and oxides). Wager's compositions, however, lie too far from the Ol-Aug boundary to represent a realistic approximation of the low-pressure Skaergaard magma evolution. The simple mass-balance approach that *Wager* [1960] proposed is not consistent with phase equilibria constraints.

Systematic differences observed between the calculated residual liquid compositions for LZa/LZb and LZc to UZa (which are unlikely to reflect fractional crystallization) are

within the accuracy of the phase equilibria used in the model. If one examines the T-X diagrams in Figures 11–13, one is easily convinced that the liquid lines of descent at temperatures below 1100°C may be changed dramatically. For example, CaO contents in the calculated liquids may differ of 2 to 2.5 wt.% in a temperature range of 10°C. Nevertheless, we cannot exclude the possibility that the compositional differences discussed above could be the geochemical effects of a late-stage process involving migration and re-equilibration of interstitial liquids.

A remarkable feature of geochemical thermometry is its ability to estimate original modal proportions of the primary liquidus minerals and residual liquid. The results summarized in Figure 10 are in fairly good agreement with the observed mineralogical assemblages that define the main units of the Layered Series. Estimated amounts of interstitial melt range around 50 wt.%. I believe that estimate is correct for the rocks of LZa and LZb, but it may be underestimated by 10 to 20 wt.% for gabbros with abundant magnetite and ilmenite owing to a slightly over-estimated (up to 10°C) initial rock formation temperatures.

Finally, our interpretations of the results of phase equilibria modelling depend upon the accuracy of the COMAGMAT calculations. The problems we have outlined indicate that even careful calibrations giving a precision of ±10°C may be insufficient to give unambiguous conclusions, especially when dealing with multi-phase assemblages including 5–6 minerals plus melt. This does not mean we are not confident of the utility of magma crystallization models. Despite the difficulties we have oulined, systematic phase equilibria modelling of intrusive rocks can be a controlling factor allowing petrologists to surmount the inadequacies of other techniques, such as mass-balance calculations. In the context of modelling the Skaergaard rocks, the most serious need are experimental data on the melting relations of magnetite and ilmenite in assemblages spanning the unexplored range of Fe-Ti rich and silica depleted compositions (Figure 4d). These data could be used in the future for more accurate calibrations of COMAGMAT and other magma crystallization models.

Appendix A: Method of Geochemical Thermometry

This method is based on the premise that any crystal-liquid mush that produces a completely crystalline rock should pass through a stage when relative motions of solids

and interstitial liquid have ceased, so that the system may be considered as closed. In this case, it is theoretically feasible to calculate all thermodynamic parameters for the initial system, using phase equilibria models designed for the calculation of equilibrium melting/crystallization relations in igneous rocks. Like the other methods, this approach entails certain assumptions as to the mechanisms of differentiation of intrusive rocks.

A.1. Basic Principles and Definitions

If crystals grew to sufficiently large sizes before settling to the floor, then the interstitial liquid would have approximately the same major- and trace-element concentrations as the liquid constituting the main part of convecting magma in which they were accumulated. This is also true if the crystals nucleated and grew *in situ*, with the residual liquid being exchanged by chemical diffusion with the main magma body. In both cases the average phase composition for the rock at any particular horizon may be given by the expression:

$$\sum_{j=1}^{M} F_j^{cr} + F_l^{in} = 1 \ , \tag{A.1}$$

where F_j^{cr} and F_l^{in} are initial modal proportions of a particular mineral $j (1 \leq j \leq M)$ and interstitial liquid (l). The bulk chemical composition of such a crystal mush is expressed as:

$$C_i^r = F_l^{in} C_i^{l(0)} + \sum_{j=1}^{M} F_j^{cr} C_i^{j(0)} \ , \tag{A.2}$$

where $C_i^{l(0)}$ is the interstitial liquid composition, whereas $C_i^{j(0)}$ should be attributed to average weighted contents of element i in mineral j accounting for a range of original compositions for each particular mineral.

The physical history of the formation of a rock from the crystal mush may be consistent with "closed" and "open" system evolution. The first situation means that cooling of the heterogeneous layer results in simple chilling (contact rocks), or interstitial crystallization with new minerals precipitated from the liquid matrix (orthocumulates). It is also possible that primary crystals undergo some amount of additional growth at the expense of the interstitial melt, followed by crystallization of the residual matrix. In all cases closed systems conserve the whole composition given by Equation (2), even though the compositions of individual primocrysts and interstitial material may change. The primary "trapped melt" temperature may be called by the formation temperature of the magmatic rock in the geochemical sense that the bulk rock composition did not change during further cooling. If so, F_j^{cr} and F_l^{in} should be treated as initial or *original modal proportions,* with $C_i^{j(0)}$ representing original mineral compositions [*Ariskin and Barmina,* 2000; *Barmina et al.,* 1989a].

In "open" systems the original modal proportions may change by later growth or compaction of the crystals (increasing F_j^{cr}) and the accompanied exclusion of part of the initial interstitial liquid (decreasing F_l^{in}). In addition, liquid percolation may give rise to a compositional re-equilibration of the initial primocrysts and migrating melts and significant modification of the initial bulk compositions, C_i^r. Nevertheless, in all of the open systems one can conceive of a stage when transport events cease. Beginning from this point, the percolating system is closed [*Hunter,* 1996], so that its whole chemistry defines the composition of the rock to be formed further in situ. It means that bulk modal and chemical compositions of the rocks produced during open system evolution can be also expressed by Equations (1, 2), but genetic interpretations of the values $F_j^{cr}, F_l^{in}, C_i^{j(0)}$, and $C_i^{l(0)}$ must attribute them to one or more dynamic, probably late-stage, processes of reorganization.

A.2. Main Assumptions

If we assume the whole rock chemistry contains a record of the original rock formation parameters, there is the possibility of extracting such genetic information. Two main assumptions should be done to resolve the problem. The most important is that the liquid and crystals were in chemical equilibrium, with the formation temperature as an intensive parameter of the equilibrium. The second assumption is that there are samples having bulk compositions different from each other only due to variations of the modal proportions F_j^{cr} and F_l^{in}, with the "trapped" liquid and temperature being the same.

If both assumptions are true, one can state that during equilibrium melting of samples having the same "formation temperature" the modelled liquid lines of descent will converge with falling temperature and intersect at a point in temperature-compositional space that represents the conditions under which the assemblage was formed [*Frenkel et al.,* 1988a, 1988b]. Failure to find such an intersection would indicate the absence of the local thermodynamic equilibrium and a link between the values for $C_i^{j(0)}$ and $C_i^{l(0)}$. Thus, to decipher the genetic record of the rock it is necessary: (1) to select a group of samples for which one would expect the initial formation conditions to have been the same, (2) to conduct a series of physical or numeric equilibrium melting experiments for these samples, (3) to determine or calculate the chemical evolution of modelled liquids, (4) to construct T-X lines of this evolution for each sample and to identify the intersection point. In some aspects the approach is similar to the method of isotope geochronology in which an isochron is constructed by searching for an intersection point corresponding to the ages of the last isotopic equilibrium for both rocks and minerals [*Ariskin and Barmina,* 2000].

In practice, the method of geochemical thermometry is accomplished by means of the COMAGMAT phase equilibria model [*Ariskin,* 1999; *Ariskin et al.,* 1993]. Although the program was primarily designed to simulate fractionation of basaltic magmas, it can also be used to calculate the course of equilibrium crystallization both for melts and cumulus rock compositions. Because equilibrium crystallization is reversible with respect to equilibrium melting, the construction of "melting" lines can be replaced with the crystalliza-

tion trajectories for starting compositions identical to those of the rocks under consideration. Applying the method to natural assemblages, one should account for both analytical and computational uncertainties that yield formation temperatures with a determined error. As a rule, instead of an ideal intersection point (for a small number of modelled lines their convergence for each petrogenic oxide can be determined visually) one can see on the T-X diagrams a compact cluster of liquids lines of descent closing on one another in a range of 10–20°C that corresponds to the accuracy of the COMAGMAT model [Ariskin, 1999]. Our experience in the phase equilibria calculations for dolerites and diabases from differentiated sills [Barmina et al., 1989a, 1989b; Frenkel et al., 1989; Krivolutskaya et al., 2001], gabbros and troctolites from the Partridge River intrusion [Chalokwu et al., 1993, 1996] and large layered complexes [Ariskin et al., 2003; Barmina and Ariskin, 2002] has shown that the greater the contrast in compositions that are used, the more accurate the estimates of the trapped (interstitial) liquid temperature and composition that are obtained. This is confirmed by the results obtained for the rocks of the Skaergaard Marginal Border Series (Figure 2).

The results presented in this paper indicate that the determination of formation temperatures graphically, based on intersections of the modelled T-X trajectories (Figures 8–13), is somewhat subjective, because the approximate uncertainties of 10–15°C for this approach are close to the cited internal calibration accuracy of the COMAGMAT model. However, one must take into account the fact that the Layered Series rocks are differentiated. This imposes a set of important limitations on how one determines the original temperature and liquid composition for each sample: (1) the calculated and observed "cumulus" mineral assemblage must correspond, (2) the modelled mineral compositions should be close (as much as possible) to those observed in selected rocks; and (3) melts entrapped in cumulates from higher levels of the Layered Series should represent lower temperature melts compared to those from underlying zones. Thus, the average values given in Table 4 were calculated for clusters of modelled T-X lines determined according to the petrologic restrictions given above. This does not allow one to specify strictly the accuracy of each calculated thermodynamic parameter, but provides an internally consistent approximation of T, $\log fO_2$, liquid component concentrations, mineral compositions, and original modal proportions.

Appendix B: Special Calibration of COMAGMAT

The COMAGMAT programs rely upon mineral-melt equilibria geothermometers for olivine, plagioclase, augite, pigeonite, orthopyroxene, titaniferous magnetite, and ilmenite appropriate for a wide range of fO_2 (from IW to $NNO+1$ buffers) and pressures from 1 atm to 10–15 kbar [Ariskin, 1999]. These semi-empirical dependencies were derived from a large dataset of experiments carried out mostly in tholeiitic systems covering compositions ranging from basalt to

dacite. The general precision of phase equilibria calculations is about 10 to 15°C and 1 to 3 mol. % for each individual mineral. With such uncertainties, the use of mass-balance constraints in the COMAGMAT-3.5 model allows one to calculate equilibrium liquid compositions with an accuracy of 0.1 to 1 wt.%, which varies for different components and depends on the modal proportions between the melt and solids [Ariskin and Barmina, 1999, 2000].

A problem of application of COMAGMAT-3.5 to the Layered Series is the relatively low temperature mineral assemblages in LZc, MZ, and UZa rocks, $\sim$1115–1080°C [McBirney, 1996]. In fact, the "silicate basis" of the COMAGMAT model was calibrated at higher temperatures of 1120–1350°C, with only a few points falling in the lower range. As a result, some calculations near 1100°C and below resulted in a shift of the modelled phase boundaries, e.g. producing an unrealistic enlargement of the Aug field at the expense of Pl and Pig. Moreover, calculated plagioclase compositions were found to be systematically more sodic and potassic than those observed in the natural assemblages. This forced me to reconsider and to modify the initial experimental dataset, drawing more attention to ferrobasaltic systems equilibrated in the vicinity of 1100°C.

To achieve this goal, we used the INFOREX experimental database [Ariskin et al., 1996, 1997], which now contains information from 290 melting experiment studies including over 10500 subliquidus runs. Searching the database for 1 atm experiments that resulted in saturation with Pl, Ol, Aug, and $Pig\pm$ oxides in the range 1050–1250°C (run duration $\geq$ 48 hours) yielded 270 experimental glass compositions containing $7 \leq FeO \leq 18$ wt.%, $45 \leq SiO_2 \leq 60$ wt.%, and $2 \leq Na_2O+K_2O \leq 5$ wt.%. For most of the glasses (which are classified as ferrobasalts to ferrodacites – Figure 4), equilibrium mineral compositions have been determined, so that four subsets of 153 points for Ol, 187 for Pl, 125 for Aug, and 43 for Pig have been formed. That mineral-melt information was processed in the manner of Ariskin et al. [1993] to develop a system of new mineral-melt geothermometers. The semi-empirical dependencies have been incorporated into COMAGMAT and tested by solving the inverse temperature-compositional problem, based on the initial dataset for each mineral. The new COMAGMAT program (version 3.65) produced a small improvement in the temperature calculations for Pl, Aug, and Pig (as compared to COMAGMAT-3.5), although modelled plagioclase compositions and phase relations between pyroxenes became more realistic. New olivine geothermometers resulted in the temperatures and compositions similar to those obtained in the older version and were left unchanged. Thus, the new "ferrobasaltic" COMAGMAT-3.65 model was used for phase equilibria calculations simulating equilibrium crystallization of the Skaergaard rocks.

References

Albarede, F., and A. Provost, Petrological and geochemical mass-balance equations: an algorithm for least square fitting and error analysis, Comput. Geosci., 3, 309–326, 1977.

Ariskin, A. A., Calculation of titanomagnetite stability on the liquidus of basalts and andesites with special reference to tholeiitic magma differentiation, *Geochem. Intern., 36,* (1), 15–23, 1998.

Ariskin, A. A., Phase equilibria modelling in igneous petrology: use of COMAGMAT model for simulating fractionation of ferrobasaltic magmas and the genesis of high-alumina basalt, *J. Volcanol. Geotherm. Res. , 90,* 115–162, 1999.

Ariskin, A. A., and G. S. Barmina, An empirical model for the calculation of spinel-melt equilibrium in mafic igneous systems at atmospheric pressure: II, Fe-Ti oxides, *Contrib. Mineral. Petrol., 134,* 251–263, 1999.

Ariskin, A. A., and G. S. Barmina, *Modelling phase equilibria at crystallization of basalt magmas* (in Russian), 363 pp., Nauka/Nauka-Interperiodica, Moscow, 2000.

Ariskin, A. A., E. D. Konnikov, and E. V. Kislov, Modelling equilibrium crystallization for ultramafic rocks as applied to problems of the phase layering formation of the Dovyren pluton (Northern Baikal, Russia), *Geochem. Intern.,* 2003 (in press).

Ariskin, A. A., G. S. Barmina, M. Ya. Frenkel, and A. A. Yaroshevsky, Simulating low-pressure tholeiite-magma fractional crystallization, *Geochem. Intern., 25,* (4), 21–37, 1988.

Ariskin, A. A., G. S. Barmina, S. S. Meshalkin, G. S. Nikolaev, and R. R. Almeev, INFOREX-3.0: A database on experimental phase equilibria in igneous rocks and synthetic systems, II, Data description and petrological applications, *Comput. Geosci., 22,* 1073–1082, 1996.

Ariskin, A. A., M. Ya. Frenkel, G. S. Barmina, and R. L. Nielsen, COMAGMAT: a Fortran program to model magma differentiation processes, *Comput. Geosc., 19,* 1155–1170, 1993.

Ariskin, A. A., S. S. Meshalkin, R. R. Almeev, G. S. Barmina, and G. S. Nikolaev, INFOREX information retrieval system: analysis and processing of experimental data on phase equilibria in igneous rocks, *Petrology, 5,* 28–36, 1997.

Barmina, G. S., and A. A. Ariskin, Estimation of chemical and phase characteristics for the initial magma of the Kiglapait troctolite intrusion, Labrador, Canada, *Geochem. Intern., 40,* (10), 972–983, 2002.

Barmina, G. S., A. A. Ariskin, E. V. Koptev-Dvornikov, and M. Ya. Frenkel, Estimates of the primary compositions of cumulate-minerals in differentiated traps, *Geochem. Intern., 26,* (3), 32–42, 1989a.

Barmina, G. S., A. A. Ariskin, and M. Ya. Frenkel, Petrochemical types and crystallization conditions of the Kronotsky Peninsula plagiodolerite (Eastern Kamchatka), *Geochem. Intern., 26,* (9), 24–37, 1989b.

Blank, H. R., and M. E. Gettings, Subsurface form and extent of the Skaergaard intrusion, East Greenland, *Trans. Amer. Geophys. Union, 54,* p. 507, 1973.

Brooks, C. K., and T. F. D. Nielsen, Early stages in the differentiation of the Skaergaard magma as revealed by a closely related suite of dike rocks, *Lithos, 11,* 1–14, 1978.

Brooks, C. K., and T. F. D. Nielsen, The differentiation of the Skaergaard intrusion, A discussion of Hunter and Sparks (Contrib Mineral Petrol 95: 451–461), *Contrib. Mineral. Petrol., 104,* 244–247, 1990.

Brooks, C. K., L. M. Larsen, and T. F. D. Nielsen, Importance of iron-rich tholeiitic magmas at divergent plate margins: a reappraisal, *Geology, 19,* 269–272, 1991.

Chalokwu, C. I., and N. K. Grant, Reequilibration of olivine with trapped liquid in the Duluth Complex, Minnesota, *Geology, 15,* 71–74, 1987.

Chalokwu, C. I., N. K. Grant, A. A. Ariskin, and G. S. Barmina, Simulation of primary phase relations and mineral compositions in the Partridge River intrusion, Duluth Complex, Minnesota: implications for the parent magma composition, *Contrib. Mineral. Petrol., 114,* 539–549, 1993.

Chalokwu, C. I., A. A. Ariskin, and E. V. Koptev-Dvornikov, Magma dynamics at the base of an evolving magma chamber: Incompatible element evidence from the Partridge River intrusion, Duluth Complex, Minnesota, USA, *Geochim. Cosmochim. Acta, 60,* 4997–5011, 1996.

Frenkel, M. Ya., A. A. Ariskin, G. S. Barmina, M. I. Korina, and E. V. Koptev-Dvornikov, Geochemical thermometry of magmatic rocks – principles and example, *Geochem. Intern., 25,* (6), 35–50, 1988a.

Frenkel, M. Ya., A. A. Yaroshevsky, A. A. Ariskin, G. S. Barmina, E. V. Koptev-Dvornikov, and B. S. Kireev, *Dynamics of in situ differentiation of mafic magmas* (in Russian), 216 pp., Nauka, Moscow, 1988b.

Frenkel, M. Ya., A. A. Yaroshevsky, A. A. Ariskin, G. S. Barmina, E. V. Koptev-Dvornikov, and B. S. Kireev, Convective-cumulative model simulating the formation process of stratified intrusions, in *Magma-crust interactions and evolution,* pp. 3–88, Theophrastus Publ. SA, Athens-Greece, 1989.

Frost, B. R., and D. H. Lindsley, Equilibria among Fe-Ti oxides, pyroxenes, olivine and quartz: Part II, Application, *Amer. Miner., 77,* 1004–1020, 1992.

Frost, B. R., D. H. Lindsley, and D. J. Anderson, Fe-Ti oxide-silicate equilibria: assemblages with fayalitic olivine, *Amer. Miner., 73,* 727–740, 1988.

Ghiorso, M. S., and I. S. E. Carmichael, Chemical mass transfer in magmatic processes II, Applications in equilibrium crystallization, fractionation and assimilation, *Contrib. Mineral. Petrol., 90,* 121–141, 1985.

Grove, T. L., Corrections to expressions for calculating mineral-components in "Origin of calc-alkaline series lavas at Medicine Lake volcano by fractionation, assimilation and mixing" and "Experimental petrology of normal MORB near the Kane Fracture Zone: 22°–25°N, mid-Atlantic ridge", *Contrib. Mineral. Petrol., 114,* 422–424, 1993.

Grove, T. L., and M. B. Baker, Phase equilibrium controls on the tholeiitic versus calc-alkaline differentiation trends, *J. Geophys. Res., 89B,* 3253–3274, 1984.

Henderson, P., The significance of the mesostasis of basic layered igneous rocks, *J. Petrol., 11,* 463–471, 1970.

Hoover, J. D., The chilled marginal gabbro and other contact rocks of the Skaergaard intrusion, *J. Petrol., 30,* 441–476, 1989.

Hunter, R. H., Texture development in cumulate rocks, in Layered intrusions, *Elsevier Science B. V., Developments in Petrology, 15,* 77–101, 1996.

Hunter, R. H., and R. S. J. Sparks, The differentiation of the Skaergaard intrusion, *Contrib. Mineral. Petrol., 95,* 451–461, 1987.

Hunter, R. H., and R. S. J. Sparks, The differentiation of the Skaergaard intrusion, Replies to A. R. McBirney and H. R. Naslund, to S. A. Morse, to C. K. Brooks and T. F. D. Nielsen, *Contrib. Mineral. Petrol., 104,* 248–254, 1990.

Jang, Y. D., and H. R. Naslund, Major and trace element composition of Skaergaard plagioclase; geochemical evidence for changes in magma dynamics during the final stage of crystallization of the Skaergaard intrusion, *Contrib. Mineral. Petrol., 140,* 441–457, 2001.

Kersting, A. B., R. J. Arculus, J. W. Delano, and D. Loureiro, Electrochemical measurements bearing on the oxidation state of the Skaergaard Layered Intrusion, *Contrib. Mineral. Petrol., 102,* 376–388, 1989.

Krivolutskaya, N. A., A. A. Ariskin, S. F. Sluzhenikin, and D. M. Turovtsev, Geochemical thermometry of the Talnakh intrusion: assessment of the melt composition and the crystallinity of the parental magma, *Petrology, 9,* 389–414, 2001.

Lindsley, D. H., G. M. Brown, and I. D. Muir, Conditions of the ferrowollastonite-ferrohedenbergite inversion in the Skaergaard intrusion, East Greenland, *Miner. Soc. Amer. Spec. Publ., 2,* 193–201, 1969.

McBirney, A. R., Differentiation of the Skaergaard intrusion, *Nature, 253,* 691–694, 1975.

McBirney, A. R., The Skaergaard Layered Series: I, Structure and average compositions, *J. Petrol., 30,* 363–397, 1989.

McBirney, A. R., Mechanism of differentiation in the Skaergaard intrusion, *J. Geol. Soc. London, 152,* 421–435, 1995.

McBirney, A. R., The Skaergaard Intrusion, in Layered intrusions, *Elsevier Science B. V., Developments in Petrology, 15,* 147–180, 1996.

McBirney, A. R., The Skaergaard Layered Series: Part V, Included trace elements, *J. Petrol., 39,* 255–276, 1998.

McBirney, A. R., and R. H. Hunter, The cumulate paradigm reconsidered, *J. Geol., 103,* 114–122, 1995.

McBirney, A. R., and Y. Nakamura, Immiscibility in late-stage of the Skaergaard intrusion, *Carnegie Inst. Wash. Yearb, 72,* 348–352, 1973.

McBirney, A. R., and H. R. Naslund, The differentiation of the Skaergaard intrusion, A discussian of Hunter and Sparks (Contrib Mineral Petrol 95: 451–461), *Contrib. Mineral. Petrol., 104,* 235–240, 1990.

Morse, S. A., Kiglapait geochemistry IV: the major elements, *Geochim. Cosmochim. Acta, 45,* 461–479, 1981.

Morse, S. A., The differentiation of the Skaergaard intrusion, A discussian of Hunter and Sparks (Contrib Mineral Petrol 95: 451–461), *Contrib. Mineral. Petrol., 104,* 240–244, 1990.

Morse, S. A., D. H. Lindsley, and R. J. Williams, Concerning intensive parameters in the Skaergaard Intrusion, *Amer. J. Sci., 280A,* 159–170, 1980.

Nikolaev, G. S., A. A. Borisov, and A. A. Ariskin, New fO_2-barometers for quenched glasses of various petrochemical series, *Geochem. Intern., 34,* (9), 753–756, 1996.

Osborn, E. F., Role of oxygen pressure in the crystallization and differentiation of basaltic magma, *Amer. J. Sci., 257,* 609–647, 1959.

Presnall, D. C., The join forsterite-diopside-iron oxide and its bearing on the crystallization of basaltic and ultramafic magmas, *Amer. J. Sci., 264,* 753–809, 1966.

Sack, R. O., I. S. E. Carmichael, M. Rivers, and M. S. Ghiorso, Ferric-ferrous equilibria in natural silicate liquids at 1 bar, *Contrib. Mineral. Petrol., 75,* 369–376, 1980.

Sato, M., and M. Valenza, Oxygen fugacities of the layered series of the Skaergaard intrusion, East Greenland, *Amer. J. Sci., 280A,* 134–158, 1980.

Snyder, D., I. S. E. Carmichael, and R. A. Wiebe, Experimental study of liquid evolution in a Fe-rich, layered mafic intrusion: constraints of the Fe-Ti oxide precipitation on the $T - fO_2$ and $T - c$ paths of tholeiitic magmas, *Contrib. Mineral. Petrol., 113,* 73–86, 1993.

Stormer J. C., Jr., The effects of recalculation on estimates of temperature and oxygen fugacity from analyses of multicomponent iron-titanium oxides, *Amer. Miner., 68,* 586–594, 1983.

Toplis, M. J., and M. R. Carroll, Differentiation of ferro-basaltic magmas under conditions open and closed to oxygen: implications for Skaergaard intrusion and other natural systems, *J. Petrol., 37,* 837–858, 1996.

Toplis, M. J., G. Libourel, and M. R. Carroll, The role of phosphorus in crystallization processes of basalt: an experimental study, *Geochim. Cosmochim. Acta, 58,* 797–810, 1994.

Tormey, D. R., T. L. Grove, and W. B. Bryan, Experimemtal petrology of normal MORB near the Kane Fracture Zone: $22°-25°N$, mid-Atlantic ridge, *Contrib. Mineral. Petrol., 96,* 121–139, 1987.

Wager, L. R., The major element variation of the layered series of the Skaergaard intrusion and re-estimation of the average composition of the hidden layered series and of the successive residual magmas, *J. Petrol., 1,* 364–398, 1960.

Wager, L. R., and W. A. Deer, Geological investigations in East Greenland, Part III, The petrology of the Skaergaard intrusion, Kangerdlugssuaq, East Greenland, *Meddelelser om Gronland, 105,* 1–352, 1939.

Wager, L. R., and G. M. Brown, *Layered Igneous Rocks,* 558 p., Oliver and Boyd, Edinburgh, 1967.

Williams, R. J., Reaction constants in the system $FeO-MgO-SiO_2-O_2$; intensive parameters in the Skaergaard intrusion, East Greenland, *Amer. J. Sci., 271,* 132–146, 1971.

Yang, H.-J., R. J. Kinzler, and T. L. Grove, Experiments and models of anhydrous, basaltic olivine-plagioclase-augite saturated melts from 0.001 to 10 kbar, *Contrib. Mineral. Petrol., 124,* 1–18, 1996.